Title: Microglia promote extracellular matrix deposition and restrict excitatory synapse numbers in the mesolimbic dopamine system during healthy aging

Authors: Daniel T. Gray[1], Abigail Guitierrez[1], Yasaman Jami- Alahmadi [2], Vijaya Pandey[2], Lin Pan[3], Ye Zhang[3], James A. Wohlschlegel[2], Lindsay M. De Biase[1]

Author Affiliations:

1. Department of Physiology, David Geffen School of Medicine, University of California, Los Angeles. Los Angeles, CA 90095
2. Department of Biological Chemistry, David Geffen School of Medicine, University of California, Los Angeles. Los Angeles, CA 90095
3. Department of Psychiatry and Biobehavioral Sciences, Semel Institute for Neuroscience and Human Behavior, David Geffen School of Medicine, University of California, Los Angeles. Los Angeles, CA 90095

Abstract

Synapse dysfunction has been definitively linked to cognitive impairments in the aging brain, and microglial physiology has emerged as a robust regulator of synapse status and cognitive aging outcomes. Hippocampal microglia have recently been shown to regulate synapse function via targeted remodeling of the extracellular matrix (ECM), yet the degree to which microglia-ECM interactions impact synapse function in the healthy aged brain remains virtually unexplored. This study combines high-resolution imaging and ECM-optimized tissue proteomics to examine the impact that microglial physiology has on ECM and synapse status in the basal ganglia of healthy aging mice. Our results demonstrate that deposition of the ubiquitous ECM scaffold hyaluronan increases during aging in the ventral tegmental area (VTA), but not its downstream target, the nucleus accumbens, and that VTA microglial tissue coverage correlates with local hyaluronan deposition. Proteomic mapping of core matrisome proteins showed prominent regional differences in ECM composition across basal ganglia nuclei that were significantly associated with abundance of chemokine receptors and synapse proteins. Finally, manipulation of microglial fractalkine signaling through Cx3Cr1 receptor deletion reversed age-associated ECM accumulation within the VTA and resulted in abnormally elevated synapse numbers in this brain region by middle age. These findings indicate that microglia promote age-related increases in ECM deposition in some, but not all, brain regions that may restrict local excitatory synapse numbers. This microglial function could represent an adaptive response to brain aging that helps to maintain appropriate activity patterns within basal ganglia circuits.

Introduction

Synapse loss and changes in plasticity are hallmark features of both normative brain aging and preclinical phases of neurodegenerative disease (e.g., Burke and Barnes, 2006; Tagliaferro and Burke, 2016; Terry et al., 1991). Regardless of age, individual differences in synaptic properties predict cognitive abilities better than most neurobiological factors, and the preservation of synapse function in healthy aged rodent and nonhuman primate brains has been linked to better cognitive outcomes (Barnes, 1979; Burke and Barnes, 2006; Dumitriu et al., 2010; Hara et al., 2012; Morrison and Baxter, 2012). Growing evidence suggests that neuroimmune status is a robust predictor of neurodegenerative disease vulnerability and age-associated cognitive decline (Felsky et al., 2019, 2018; Prater et al., 2023; Schwabe et al., 2020; Wood, 2022). Microglia, the primary brain immune cells, regulate synapse function across the lifespan through synapse engulfment and control of neuronal membrane excitability, in addition to other mechanisms (Badimon et al., 2020; Cserép et al., 2020; Lewitus et al., 2016; Miyamoto et al., 2016; Paolicelli et al., 2011; Parkhurst et al., 2013; Schafer et al., 2012; Stevens et al., 2007; Weinhard et al., 2018). This suggests that microglial regulation of synapses may critically shape patterns of age-associated cognitive decline and neurodegenerative disease susceptibility.

One recently discovered way in which microglia regulate synapse function is through targeted degradation of the brain extracellular matrix (ECM; Crapser et al., 2021; Nguyen et al., 2020; Rowlands et al., 2018; Soria et al., 2020; Venturino et al., 2021). The ECM is not static, but represents a dynamic network of proteins and carbohydrates that is remodeled in disease states, during injury and repair, and to support structural plasticity (Dityatev et al., 2010; Sorg et al., 2016). Several studies indicate that ECM composition varies substantially across brain regions in terms of its abundance (Brückner et al., 1999, 1993; Härtig et al., 1992; Hobohm et al., 1998; Lensjø et al., 2017), composition (Dauth et al., 2016; Fawcett and Kwok, 2022), and

degree of remodeling during aging (Foscarin et al., 2017; Nguyen et al., 2020; Ueno et al., 2019, 2018). In support of the idea that microglia regulate the ECM, pharmacological depletion of microglia increases cortical ECM proteoglycan abundance in aging 5xFAD mice (Crapser et al., 2020), and microglial densities are negatively correlated with perineuronal nets (specialized ECM structures) in aging macaque cortex (Gray et al., 2022). Moreover, microglial release of metalloproteinases and other ECM-degradative enzymes declines during healthy aging, resulting in excessive ECM deposition at synapses and reduced structural plasticity in the hippocampus (Nguyen et al., 2020). Collectively, these studies suggest that microglial responses to aging and disease include alterations in microglial-ECM interactions, with downstream consequences for ECM-synapse dynamics. Yet, the microglia-ECM-synapse triad remains virtually unexamined in most brain regions in young adult and aging brains.

Microglia exhibit stark regional specializations that likely influence their interactions with the ECM in young and aging brains (Ayata et al., 2018; De Biase et al., 2017; Grabert et al., 2016). Such specializations in microglial phenotype are especially prominent across nuclei of the basal ganglia dopamine system and are characterized by differences in cell density, cell morphology, and mitochondrial and lysosome-relevant gene expression (De Biase et al., 2017; Hope et al., 2020). Dysregulation of mesolimbic dopamine circuits is prominent during normative aging (Bäckman et al., 2010, 2006; Berry et al., 2016; Dahl et al., 2023) and microglia near dopamine neurons exhibit increases in proliferation and inflammatory factor production much earlier in the aging progression compared to microglia in other basal ganglia nuclei (Moca et al., 2022). Such regional specializations in microglial phenotype and responses to aging make the basal ganglia dopamine system ideal for mapping microglial-ECM interactions during aging and probing whether these interactions play key roles in determining age-dependent changes in synapse function. The present study combines high-resolution imaging and quantitative tissue

proteomics to examine relationships between synapse status, microglial aging phenotypes, and ECM deposition across the mesolimbic dopamine system.

Results

Region- and age-dependent differences in hyaluronan matrix deposition in the aging mesolimbic dopamine system

A critical, ubiquitous component of the brain ECM is the glycosaminoglycan hyaluronan, which acts as a scaffold for attachment and aggregation of proteoglycans and other glycosylated proteins. In this way, hyaluronan plays critical roles in determining the overall tissue topology of the ECM (Perkins et al., 2017; Peters and Sherman, 2020; Soria et al., 2020; Wilson et al., 2020). For an initial assessment of ECM structure in basal ganglia nuclei where microglia exhibit prominent regional specialization and distinct responses to aging, high-resolution (63x) confocal images of histochemically labeled hyaluronan were acquired in the ventral tegmental area (VTA) and nucleus accumbens (NAc) of young adult (4 months) and late-middle-aged (18 months), wild-type, C57Bl6 mice (**Figure 1A, 1B**). Hyaluronan fibril density, median size, and distribution regularity were greater in the VTA compared to NAc (ANOVA - Density: $F(1,45) = 32.18$, $p < 0.001$, **Figure 1C**; Size: $F(1,45) = 23.38$, $p < 0.001$, **Figure 1D**; Regularity: $F(1,45) = 83.07$, $p < 0.001$, **Figure 1E**). Late-middle-aged mice exhibited significantly greater VTA hyaluronan fibril density (unpaired t-test; $t(21) = 2.03$, $p < 0.049$; **Figure 1C**) and distribution regularity (unpaired t-test; $t(21) = 4.16$, $p < 0.001$, **Figure 1E**) relative to young adults. In contrast, these measures of hyaluronan matrix structure were not different between young and late-middle-aged mice in the NAc (unpaired t-test; Density: $t(21) = -.31$, $p = 0.76$; Size: $t(21) = - 0.58$, $p = 0.57$; Regularity: $t(21) = -0.57$, $p = 0.58$; **Figure 1C, 1D, 1E**). These data indicate that hyaluronan matrix structure varies substantially across basal ganglia nuclei and undergoes age-dependent modifications in the same regions where microglia show early responses to aging (Moca et al., 2022).

Abundance of core matrisome proteins differs across the midbrain and striatum of healthy aged mice

The histological analysis of a critical ECM scaffold described above indicates that there is substantial regional variation in the ECM within the basal ganglia and that the impact of aging on ECM structure also varies across regions. However, numerous additional proteins attach to hyaluronan to make up the full matrix. For unbiased and more comprehensive analysis of this "matrisome" at both ends of the adult lifespan, LC-MS/MS quantitative proteomic analysis was applied to midbrain (containing VTA) and striatal (containing NAc) tissue of young (3-4 months) and aged (22-24 months) wild-type mice (**Figure 2A**). Proteomic analysis of the brain's core matrisome has typically been hindered by the insolubility and glycosylation of ECM proteins, which make estimations of protein concentrations using traditional chaotropic digestion techniques difficult. Consequently, most ECM studies use combinations of histological and biochemical assessments of individual matrix components and are unable to assess the entire matrisome within an individual animal. Here, a tissue fragmentation and protein digestion protocol that shows efficacy for isolating ECM proteins in different tissues throughout the body (Naba et al., 2015) was applied to create the first proteomic map of the mesolimbic dopamine system during normative aging.

Core matrisome protein abundance was higher in aged mice compared to young in both soluble and insoluble tissue fractions (ANOVA; $F(1,31) = 5.32$, $p = 0.029$; **Figure 2B**). Core matrisome protein abundance was also greater in the midbrain compared to striatum (ANOVA; $F(1,31) = 7.6$, $p = 0.01$; **Figure 2B**), consistent with greater abundance of hyaluronan observed in this region histologically. Volcano plots of overall protein abundance (pooled across solubility fractions) show that most core matrisome proteins were more abundant in aged brains (positive $\log_2$(ratio)), and that similar numbers of matrisome proteins were differentially expressed during aging in the midbrain and striatum (**Figure 2C**).

Core matrisome proteins fall into 3 subclasses – collagens, glycoproteins, and proteoglycans. Examination of each subclass revealed similarities as well as differences in midbrain and striatum ECM composition and aging-induced modifications. One striking regional difference was that there were eight distinct collagens detected in the midbrain compared to just two in the striatum (**Figure 2D**). Moreover, several of these collagens increased in abundance within the midbrain during aging (**Figure 2D**). The most pronounced regional difference in ECM glycoprotein abundance with age was observed in the Laminin family of proteins, which showed significant age-related increases specifically in the striatum (unpaired t-test; Laminin-α5: $t(6) = 2.50$, $p = 0.04$; Laminin-α2: $t(6) = 3.1$, $p = 0.02$; Laminin-β2: $t(6) = 2.68$, $p = 0.03$; Laminin-gamma1: $t(6) = 3.54$, $p = 0.01$; **Figure 2E**). Finally, regional differences in ECM proteoglycans were also observed. In the midbrain, age-related increases in protein abundance were observed in 3 of the 4 major chondroitin sulfate proteoglycans (unpaired t-test; versican: $t(6) = 3.71$, $p = 0.009$, neurocan: $t(6) = 2.57$, $p = 0.04$, aggrecan: $t(6) = 3.74$, $p = 0.009$; **Figure 2F**), and 2 of 3 hyaluronan and proteoglycan link proteins (unpaired t-test: HAPLN 1: $t(6) = 2.79$, $p = 0.03$; HAPLN2: $t(6) = 11.01$, $p < 0.001$; **Figure 2F**). Many of these proteoglycans were also generally more abundant in the midbrain compared to in the striatum, in both young and aging mice. In contrast, in the striatum, the only differentially expressed proteoglycan was the basement membrane-specific heparan sulfate proteoglycan core protein (HSPG; unpaired t-test: $t(6) = 2.48$, $p = 0.04$; **Figure 2F**). These observations demonstrate that regional differences in ECM composition and ECM modulation during aging extend to all three subclasses of ECM proteins.

Nonetheless, several key similarities in the impact of aging on the ECM were shared across regions. The glycoprotein tenascin C, which is a proteoglycan link protein, decreased significantly with age in both the midbrain and the striatum (unpaired t-test; midbrain: $t(6) = -2.52$, $p = 0.04$; striatum: $t(6) = -3.8$, $p = 0.01$; **Figure 2E**). The glycoproteins Von Willebrand Factor A (VWA1; unpaired t-test; midbrain: $t(6) = 3.11$, $p = 0.02$; striatum: $t(6) = 2.85$, $p = 0.03$)

and Nidogen 2 (unpaired t-test; midbrain: $t(6) = 5.15$, $p = 0.002$; striatum: $t(6) = 4.80$, $p = 0.003$; **Figure 2E**) increased significantly with age in both midbrain and striatum. **Figure 2G** summarizes core matrisome proteins found to be significantly altered by aging in the midbrain or striatum only, as well as those that were significantly altered by aging in both brain regions.

Extracellular matrix profiles are linked with synapse function in the healthy aged basal ganglia

To relate the observed regional and age-associated changes in the matrisome with other features of the local tissue proteome, Weighted Gene Coexpression Network Analysis (WGCNA; Langfelder and Horvath, 2008)) was used for unsupervised clustering and unbiased identification of protein expression patterns. This analysis identified 12 modules of covarying proteins (non-grey modules; **Figure 3A**). The majority of core matrisome proteins (~82%) were members of either the yellow, brown, or tan modules and most innate immune proteins were members of the turquoise module (33%), yellow module (15%), or brown module (12%), highlighting these modules as warranting further analysis. Examination of module eigengenes for these 4 modules revealed stark regional differences between the midbrain and striatum for the brown, yellow, and tan modules that were not present for the turquoise module (**Figure 3B**). Pathway analysis (Metascape) was used to identify biological processes associated with each module (**Figure 3C**). The brown module was enriched in proteins associated with numerous metabolic processes, neuron projection development, and cell junction organization. Yellow module proteins were associated with the regulation of various aspects of chemical synaptic transmission and synapse structure. Proteins in the tan module were associated with metabolic pathways, insulin receptor signaling, and extracellular matrix organization. Finally, the turquoise module was enriched in proteins associated with RNA and amide metabolism, regulation of translation, and membrane trafficking.

Additional pathway analysis focused on module proteins that were significantly altered by age revealed clusters of proteins in the brown/yellow/tan modules associated with ECM

organization, ECM-receptor interactions and synapse organization ($p < 0.05$; **Figure 3D, 3E**). These clusters of proteins were directly interconnected, meaning that functional annotation predicts that these ECM proteins and specific synaptic proteins can interact with and/or influence one another. Age-modulated proteins from the brown/yellow/tan modules also included proteins associated with neutrophil degranulation and fatty acid metabolism, but these proteins are not predicted to have direct functional interactions with ECM- and synapse-relevant proteins. Although similar functional annotations were observed in both the midbrain and striatum, a greater number of brown/yellow/tan module proteins were altered with aging in the midbrain (**Figure 3F**).

Pathway analysis of significantly altered proteins in the turquoise module revealed a group of proteins associated with antibody-mediated complement system activation (C1qA, C1qB, C1qC, C1qBP, C9) in the midbrain that was not observed in the striatum (**Figure 3G, 3H**). This included proteins implicated in microglial pathogen phagocytosis and synapse pruning. No clusters of proteins were shared between the midbrain and striatum, suggesting that while there were no regional differences in the abundance of turquoise module proteins (**Figure 3B**), the impact of brain aging uniquely modifies turquoise module proteins in the two regions. Again, roughly twice as many turquoise module proteins were altered during aging in the midbrain compared to striatum (**Figure 3I**). These observations indicate that complement system activation is more prominent in the aging midbrain than striatum.

Synapse status is associated with ECM proteoglycan abundance in the aging mesolimbic dopamine system

The analysis above suggests that there are key regional differences in the status of ECM proteins, synaptic proteins, and complement proteins across the midbrain and striatum. It further suggests that the status of synaptic proteins is more tightly linked to status of local ECM than local complement signaling. To evaluate these relationships further, the abundance of specific

ECM, synapse, and complement proteins were treated as “traits” and the degree to which each “trait” is correlated with module eigengenes across samples was assessed. Abundance of the hyaluronan binding proteins HAPLN1-4 each showed significant relationships with brown, yellow, tan modules supporting the idea that hyaluronan plays a prominent role in orchestrating the behavior of the overall matrisome (**Figure 4A**). Negative correlations between HAPLNs and the yellow module, which was most enriched in proteins associated with chemical synaptic transmission and synapse structure, suggests that greater hyaluronan matrix abundance may restrict synapse protein abundance. In contrast, complement proteins C1qA and C1qB exhibited significant correlations with the turquoise module eigenegene and no significant relationships with the brown/yellow/tan module eigengenes (**Figure 4A**), again suggesting that local complement deposition is not related to local ECM deposition. Abundance of numerous excitatory and inhibitory synaptic proteins were also significantly associated with brown/yellow/tan module eigengenes ($p < 0.05$), whereas no synapse proteins showed significant correlations with turquoise module eigengenes (**Figure 4B, 4C**). These observations suggest that regional variation in ECM status plays a more critical role in regulating regional differences in synapse status than complement system signaling.

Direct examination of excitatory and inhibitory synapse protein abundance revealed that the majority of individual synaptic proteins did not differ between young-adult and aged mice. Exceptions include Homer2, which was decreased significantly in the aged striatum (unpaired t-test; $t(6) = -2.88$, $p = 0.03$; **Figure 4D**). A similar non-significant trend was observed in the midbrain (unpaired t-test; $t(6) = -1.96$, $p = 0.08$; **Figure 4D**). Abundance of the metabotropic glutamate receptor subunit mGluR1 also decreased significantly in the aged midbrain (unpaired t-test; $t(6) = -2.74$, $p = 0.03$), whereas abundance of the NMDA receptor subunits GluN-1 and GluN-2A increased significantly in the aged striatum (unpaired t-test; GluN-1: $t(6) = 2.8$, $p = 0.03$; GluN-2A: $t(6) = 2.74$, $p = 0.03$; **Figure 4D**). No significant age-associated differences in

inhibitory synapse protein abundances were observed in either the midbrain or striatum (**Figure 4E**). These findings suggest that, in these brain regions and at these ages, substantial loss of functional synapses is not occurring. Furthermore, the close association between synaptic protein "traits" and ECM-prominent protein modules (**Figure 4B,4C**), as well as links between ECM status and synapse status among proteins significantly altered during aging (**Figure 3D-3F**) supports the idea that ECM abundance in the healthy aging brain plays a key role in maintaining stable numbers of synapses across the lifespan.

Hyaluronan deposition patterns correlate spatially with microglial tissue coverage

Microglia express numerous receptors that could mediate direct "sensing" of the local matrix, multiple degradative enzymes that can impact ECM components, and a potential capacity to synthesize some ECM components (Crapser et al., 2021; Tewari et al., 2022). Microglia also possess multiple mechanisms for regulating synapse status (Basilico et al., 2019; Gunner et al., 2019; Paolicelli et al., 2011; Schafer et al., 2012), including via modification of the ECM (Nguyen et al., 2020). To begin exploring how the state of basal ganglia microglia relates to local ECM and synapse structure, tissue from young (3-4 months), middle-aged (12-17 months) and aged (18-22 months) Cx3Cr1$^{EGFP/+}$ mice, which enable precise visualization of microglial morphology, was analyzed. Tissues were histochemically labeled for hyaluronan, and spatial correlations between these signals and EGFP+ microglia were examined in 20x confocal images (**Figure 5A, 5C, 5E**). In the VTA, field-of view microglial tissue coverage was significantly correlated with greater hyaluronan matrix deposition across ages (Robust regression; $t(44) = 4.45$, $p < 0.001$; **Figure 5B**). This relationship was also significant in both young and aged mice when individual age groups were assessed separately (Robust regression; young: $t(13) = 2.65$, $p = 0.02$; middle-aged: $t(12) = 1.81$, $p = 0.09$; aged: $t(13) = 2.86$, $p = 0.012$; **Figure 5B**). Microglia densities were also significantly associated with greater hyaluronan matrix deposition, (Robust regression; $t(44) = 2.57$, $p = 0.013$; **Figure 5B**), and this

relationship was also significant when analyzing only the aged mice (Robust regression; young: $t(13) = 0.87$, $p = 0.4$; middle-aged: $t(12) = 1.25$, $p = 0.23$; aged: $t(13) = 2.19$, $p = 0.045$; **Figure 5B**). In contrast, in the NAc, microglia tissue coverage and hyaluronan abundance showed no relationship at any age (Robust regression; All: $t(43) = 0.1$, $p = 0.92$; Young: $t(12) = 0.34$, $p = 0.74$; Middle-Aged: $t(12) = 0.44$, $p = 0.67$; Aged: $t(15) = 0.57$, $p = 0.57$; **Figure 5D**). Generally, NAc microglia densities were also not associated with hyaluronan deposition (Robust regression; $t(43) = 1.04$, $p = 0.3$; **Figure 5D**), although a significant positive relationship between microglia density and hyaluronan deposition was observed in young mice (Robust regression: Young: $t(12) = 2.18$, $p = 0.049$; Middle-Aged: $t(12) = -0.08$, $p = 0.94$; Aged: $t(15) = -0.61$, $p = 0.55$; **Figure 5D**).

Since variation in hyaluronan matrix distribution was evident even within a field of view, more localized analysis of hyaluronan-microglia relationships was carried out by overlaying a 10x10 grid on each 20x confocal image. The abundance of the hyaluronan and GFP signals within each square of the grid was quantified and grid values were plotted to obtain a correlation coefficient for each 20x confocal image (**Figure 5E**). Correlation coefficients between hyaluronan and microglia tissue coverage were between $r = 0.4$ and $r = 0.75$ in the VTA of young adult (3-4 months), middle-aged (12-15 months), and aged (17-24 months) mice, and did not differ with age (ANOVA $(F,2,15) = 0.12$, $p = 0.89$; **Figure 5F**). Correlation coefficients between NAc microglia and hyaluronan coverage were between $r = -0.1$ to $r = 0.3$ in young mice and increased to between $r = 0.25$ and $r = 0.78$ in middle-aged and aged mice (ANOVA; $t(2,15) = 4.88$, $p = 0.26$; unpaired t-test: young-middle aged: $t(8) = 2.8$, $p = 0.023$; young-aged: $t(9) = 2.63$, $p = 0.027$; **Figure 5F**). However, overall hyaluronan-microglia spatial correlations remained significantly lower in the NAc compared to the VTA (ANOVA; $t(1,31) = 15.98$, $p < 0.001$; **Figure 5F**). These data suggest that local microglial status impacts hyaluronan matrix distribution patterns, or vice versa.

Given the high correlation between local tissue coverage of VTA microglia and hyaluronan deposition, 63x confocal images and reconstruction of microglia and hyaluronan was carried out in Imaris to determine whether VTA microglia make direct contact with the hyaluronan matrix (**Figure 5G**). VTA microglia in young mice made relatively regular putative contacts with hyaluronan fragments, both along their processes and proximal to microglial somas. Quantification of the density of hyaluronan contacts normalized to GFP signal revealed an age-associated decrease in microglia-hyaluronan contacts in the VTA (ANOVA; $F(2,15) = 5.53$, $p = 0.019$; **Figure 5H**). The size of hyaluronan fibrils in contact with microglia was not different with age, however (ANOVA; $F(2,15) = 0.55$, $p = 0.59$; **Figure 5I**). This raises the intriguing possibility that loss of ability of VTA microglia to interact directly with hyaluronan networks is related in some way to greater hyaluronan deposition within the tissue.

Microglia regulate ECM abundance and excitatory synapse numbers in the aging VTA

The ECM has been shown to regulate various aspects of synapse function through direct ECM-synapse interactions and by regulation of neuronal excitability patterns that influence plasticity thresholds (Dityatev et al., 2010; Nguyen et al., 2020). To relate hyaluronan matrix structures to local synapse status, densities of Homer2, a postsynaptic excitatory synapse protein, were quantified in the VTA and NAc (**Figure 6A**). Homer2 densities were greater in the NAc compared to the VTA (ANOVA; $F(1,31) = 123.9$, $p < 0.001$; **Figure 6B**), but were not different between young adult and late-middle-aged mice in either the VTA (ANOVA; $F(1,15) = -0.1.55$, $p = 0.24$; **Figure 6B**) or NAc (ANOVA; $F(1,15) = -0.74$; $p = 0.41$; **Figure 6B**), consistent with proteomics data suggesting minimal overt synapse loss in these brain regions at these ages (**Figure 4D,E**).

To further assess the contribution of microglia to hyaluronan deposition and excitatory synapse numbers, the VTA and NAc of young adult (3-4 months) microglia-deficient mice were histochemically examined. Microglial deficiency was achieved via deletion of the fmrs-intronic

response element (FIRE) within the Csfr1 locus (Csf1r$^{\Delta FIRE/\Delta FIRE}$) (Rojo et al., 2019; **Figure 6C, 6D**). As in wild-type mice, hyaluronan densities were greater in the VTA than the NAc (ANOVA; $F(1,11) = 32.85$, $p < 0.001$; **Figure 6E**). However, compared to control mice, Csf1r$^{\Delta FIRE/\Delta FIRE}$ mice exhibited higher hyaluronan densities in the VTA (unpaired t-test; $t(4) = 5.03$, $p = 0.007$**; Figure 6E**), similar to what was observed in aging wild-type mice (**Figure 1**). Absence of microglia did not alter hyaluronan fibril densities in the NAc (unpaired t-test; $t(4) = 1.11$, $p = 0.33$; **Figure 6E**). Notably, a significant region-by-genotype interaction in hyaluronan density was observed (ANOVA; $F(1,11) = 5.88$, $p = 0.04$), suggesting that microglia differentially regulate hyaluronan matrix deposition patterns in the VTA and NAc. As was observed in wild-type mice, excitatory synapse densities were significantly higher in the NAc compared to the VTA in Csfr1$^{+/+}$ and Csf1r$^{\Delta FIRE/\Delta FIRE}$ mice (ANOVA; $F(1,11) = 69.99$, $p < 0.001$; **Figure 6F**). However, Homer2 puncta densities were not different between Csfr1$^{+/+}$ and Csf1r$^{\Delta FIRE/\Delta FIRE}$ mice in either the VTA or NAc (unpaired t-test; VTA: $t(4) = -0.53$, $p = 0.63$; NAc: $t(4) = 0.87$, $p = 0.44$; **Figure 6F**). All together, these observations suggest that microglia attenuate ECM deposition in the VTA, and this microglial function may be diminished with aging. While this elevated hyaluronan deposition was not associated with changes in excitatory synapse numbers in either aging wildtype mice or microglia-deficient mice, these hyaluronan changes are likely to alter proteoglycan deposition around synapses and modify capacity for structural remodeling of synapses.

CX3CR1 deficiency has been suggested to accelerate microglial aging (Gyoneva et al., 2019; Moca et al., 2022) and impact synaptic plasticity (Basilico et al., 2019; Gunner et al., 2019; Kim et al., 2020). In other bodily tissues, CX3CR1 signaling has also been shown to impact both ECM synthesis and ECM degradation (Rivas-Fuentes et al., 2020; Song et al., 2013). To explore whether CX3CR1 signaling impacts ECM-synapse interactions, hyaluronan and Homer2 were analyzed in young (3-4 months) and middle-aged (12-15 months) Cx3Cr1-het (*Cx3Cr1*$^{EGFP/+}$) and Cx3Cr1-knockout (*Cx3Cr1*$^{EGFP/EGFP}$) mice (**Figure 6G, 6H**). In both

genotypes, hyaluronan fibril densities were higher in the VTA compared to the NAc (ANOVA; $F(1,31) = 152.51$, $p < 0.001$; **Figure 6I**), as observed in wild-type mice. However, Cx3Cr1-knockout mice exhibited lower hyaluronan fibril densities in the VTA compared to Cx3Cr1-het mice (ANOVA; $F(1,15) = 5.59$, $p = 0.035$; **Figure 6I**). Surprisingly, VTA hyaluronan fibril densities were lower in middle-aged mice compared to young for both genotypes (ANOVA; $F(1,15) = 9.45$; $p = 0.009$; **Figure 6I**), which is the opposite of what was observed in aging wildtype mice. This finding suggests that, while microglia in aging wildtype mice shift toward a state that allows increased hyaluronan deposition, deficiency in Cx3Cr1 signaling pushes them into a state that actively reduces hyaluronan deposition, perhaps a hyper-phagocytic state. In the NAc, hyaluronan fibril densities were not different as a function of age or genotype (ANOVA; Age: $F(1,15) = 0.68$, $p = 0.42$; Genotype: $F(1,15) = 0.83$, $p = 0.38$; **Figure 6I**).

In both Cx3Cr1-het and Cx3Cr1-knockout mice, homer2 puncta densities were higher in the NAc compared to VTA (ANOVA; $F(1,31) = 59.04$; $p < 0.01$; **Figure 6L**), consistent with findings in wild-type mice. Intriguingly, within the VTA Cx3cr1-knockout mice had more excitatory synapses in middle age compared to Cx3Cr1-het mice (ANOVA; $F(1,15) = 11.17$, $p = 0.006$; post-hoc t-test: $t(6) = 3.04$, $p = 0.023$; **Figure 6L**). Homer2 puncta densities were not different as a function of age or genotype in the NAc (ANOVA; Age: $F(1,15) = 0.03$, $p = 0.86$; Genotype: $F(1,15) = 0.67$, $p = 0.42$; **Figure 6L**). Together these results indicate that deficits in microglial Cx3Cr1 receptor signaling reduce hyaluronan matrix deposition during aging, and these changes are associated with higher excitatory synapse numbers in the VTA by middle age. This pattern differs from the phenotype observed in middle-aged wild-type mice where synapse numbers remained stable alongside increases in hyaluronan matrix abundance.

Hyaluronan, microglia, and synapse properties are similar between male and female mice

Sexual dimorphism in numerous aspects of immune function have been demonstrated across the lifespan (Klein and Flanagan, 2016; Mangold et al., 2017). Therefore, potential sex

differences in hyaluronan, microglia, and excitatory synapse status were evaluated. Hyaluronan fibril density, size, and distribution regularity were not different as a function of biological sex (ANOVA; Density: $F(1,45) = 1.95$, $p = 0.17$; Size: $F(1,45) = 1.59$, $p = 0.21$; Regularity: $F(1,45) = 0.49$, $p = 0.49$; **Figure 1C, 1E**). Similarly, Homer2 puncta densities were similar between male and female mice (ANOVA; VTA: $F(1,15) = 2.78$, $p = 0.12$; NAc: $F(1,15) = 0.02$, $p = 0.88$; **Figure 6B**). Correlation coefficients between hyaluronan and microglia tissue coverage were not different between male and female mice (ANOVA; VTA: $F(1,15) = 1.03$, $p = 0.33$); NAc: $F(1,15) = 0.37$, $p = 0.55$; **Figure 5H**), and microglia-hyaluronan contact densities and sizes were also not different as a function of biological sex (ANOVA; Density: $F(1,15) = 0.92$; $p = 0.36$; Size $F(1,15) = 0.87$, $p = 0.37$; **Figure 5H, 5I**).

Discussion

Numerous deficits associated with normative brain aging implicate dysfunction in the mesolimbic dopamine system (Bäckman et al., 2006; Berry et al., 2016; Dahl et al., 2023), and microglia, the primary immune cell of the brain parenchyma, exhibit accelerated aging phenotypes in the VTA that have been proposed to impact dopamine circuit function. The findings in this study indicate that age-associated increases in ECM deposition patterns occur alongside VTA microglial aging phenotypes and are associated with stable excitatory synapse numbers. Perturbations of microglial Cx3Cr1 receptor signaling reduced ECM deposition and was accompanied by excess numbers of excitatory synapses. Together these observations suggest that healthy microglial aging phenotypes in the mesolimbic dopamine system may help orchestrate adaptive or compensatory responses characterized by greater ECM deposition that works to maintain synaptic drive across the healthy adult lifespan. This study provides critical observations that implicate glial-matrix interactions in differentiating healthy versus pathological brain aging states and identifies potential mechanisms by which the healthy aging brain works to maintain synaptic and neuronal network excitability patterns relatively constant across the lifespan.

Increased ECM deposition is associated with stable excitatory synapse numbers in the aged ventral tegmental area

The ECM can regulate synapse function through direct ECM-synapse interactions, control of extracellular ion concentrations, and by regulating access of phagocytic cells to synaptic elements (Soles et al., 2023; Soria et al., 2020; Tewari et al., 2022). Here we show that age-associated increases in VTA hyaluronan abundance (**Figure 1**) arise alongside no change in Homer2 densities or deposition of hyaluronan at excitatory synapses (**Figure 6B, 6C**). Multiple lines of evidence indicate that inverse relationships exist between ECM abundance and synapse stability that can either be beneficial or detrimental depending on the context. For

example, under healthy physiological conditions microglia respond to neuronal cytokines with targeted release of matrix metalloproteinases and similar degradative enzymes that locally degrade ECM proteoglycans to facilitate structural plasticity (Nguyen et al., 2020). On the other hand, degradation of ECM proteoglycans results in diffusion of AMPA receptors from postsynaptic active zones and instability in extracellular plasticity-associated proteins such as neuronal pentraxins (Chang et al., 2010; Frischknecht et al., 2009; Frischknecht and Gundelfinger, 2012). Enzymatic removal of hyaluronan in particular has been shown to elevate neuronal network excitability in 3-dimensional cortical spheroid systems by increasing excitatory synapse numbers and decreasing inhibitory synapse numbers (Wilson et al., 2020). In this study we demonstrate that the NAc has significantly more excitatory synapses compared to the VTA and that hyaluronan levels show the opposite regional trend. This may implicate that the NAc is a more malleable network as the ECM is generally thought to restrict plasticity since, for example, the closing of the developmental critical period is associated with drastic increases in ECM abundance across the brain (Lensjø et al., 2017; Pizzorusso et al., 2006, 2002; Rowlands et al., 2018). Furthermore, it may suggest that despite numbers of excitatory synapses in the VTA not changing with advanced age, these synapses may be more rigid compared to VTA synapses in younger animals.

Alterations in neuronal network excitability have been observed across numerous neuronal circuits in healthy and pathological brain aging contexts, and these changes have been linked to plasticity deficits and age-associated cognitive decline (Burke and Barnes, 2006; Haberman et al., 2017; Kaczorowski and Disterhoft, 2009; Norris et al., 1996; Oh et al., 2010; Wilson et al., 2005). Evidence from mouse models of Alzheimer’s and Parkinson’s disease, as well as brain tissue from human patients, indicates that ECM structures are less abundant in the diseased brain (Baig et al., 2005; Crapser et al., 2020; Soria et al., 2020). Similar reductions in ECM abundance have also been observed in certain vulnerable regions of the healthy aged

brain including the hippocampus and retrosplenial cortex, although many more brain regions do not exhibit these differences (Gray et al., 2023, 2022; Ueno et al., 2019, 2018). The present observation that greater hyaluronan abundance in the VTA occurred alongside no change in excitatory synapse networks may therefore reflect an adaptive or compensatory response engaged to help maintain synaptic drive onto dopamine neurons within a healthy physiological range. If increased hyaluronan matrix abundance does have the effect of making these synapses more rigid, as discussed above, then this response may reflect a tradeoff that the aging brain must make to avoid more drastic circuit dysfunction in the VTA.

Proteomic analysis reveals key regional differences in matrisome composition in the aging brain

To our knowledge, this report presents the first comprehensive proteomic mapping of brain ECM composition during healthy aging and reveals several key regional differences in ECM status in the aging midbrain and striatum. First, more ECM proteoglycans were detected in the midbrain compared to the striatum, and a greater number of proteoglycans were significantly more abundant in the midbrain. Of note, hyaluronan binding proteins (HAPLN1-4), which anchor proteoglycans to hyaluronan scaffolds, were increased in the aged midbrain, and not in the striatum. The HAPLN2 isoform, which is enriched in hindbrain regions including the midbrain compared to the cerebral cortex (Hirakawa et al., 2000; Wang et al., 2019), exhibited the greatest age-associated increase in abundance with over a 3-fold increase. This further confirms that healthy brain aging is associated with an accumulation of the hyaluronan matrix (Cargill et al., 2012; Sugitani et al., 2021; **Figure 1**) and suggests that the midbrain is particularly impacted by this change compared to other regions.

The only core matrisome protein to exhibit decreases in abundance with age was the proteoglycan link protein tenascin C. Tenascins are multimeric ECM proteins that modulate cell adhesion throughout the body, and in the brain these proteins are thought to stabilize interactions between elements of the ECM (Chiquet-Ehrismann, 2004; Mueller-Buehl et al.,

2022; Suttkus et al., 2014). Tenascin-C deficient mice exhibit impairments in hippocampal plasticity and abnormal axon conductance velocities (Evers et al., 2002; Weber et al., 1999), suggesting this protein plays important roles in regulating neuronal network functioning. Tenascin-C promotes cellular tension and regulates various other mechanical properties of the ECM (Midwood and Schwarzbauer, 2002; Miroshnikova et al., 2016; Saupe et al., 2013). Mechanosensitive ion channels like Piezo receptors, which microglia express, respond to mechanical activation with changes in Ca^{++} ion influx that alter intracellular second messenger pathways (Procès et al., 2022; Zheng et al., 2023), and this signaling axis has been shown to promote microglia phagocytosis of amyloid plaques (Hu et al., 2023). The observation that tenascin C was the only matrisome protein to significantly decrease in the aged midbrain and striatum may suggest that it is a driver of secondary increases in other ECM protein and hyaluronan abundance, possibly through changes in mechanical signaling associated with tenascin deficiency.

A greater number of ECM collagens were detected in the midbrain compared to striatum. Brain collagens have been shown to interact with hyaluronan and HAPLNs in the developing brain to modulate tissue stiffness properties (Long et al., 2018), which may suggest that the greater abundance of collagen in the midbrain is directly associated to regional differences in hyaluronan abundance. Collagen alpha-2 isoforms, which are associated with the basement membrane of brain vasculature (Kuo et al., 2012; Neyazi et al., 2020), were found to be more abundant with age in both brain regions and may reflect neurovascular dysfunction that is known to arise during brain aging (Banks et al., 2021; Verheggen et al., 2020). Finally, laminin glycoproteins were initially found at lower levels in the striatum but were significantly increased during aging compared to the midbrain. Laminins are also a key structural component of the ECM basement membrane (Hamill et al., 2009; Iorio et al., 2015), suggesting that age-associated neurovascular deficits in the midbrain and striatum may arise from distinct

mechanisms. Alternatively, our histological data suggests that the abundance of striatal hyaluronan is much lower compared to the midbrain (**Figure 1**), and since hyaluronan also localizes to brain vasculature (Reed et al., 2019, 2017), increased laminin abundance in the aged striatum may help stabilize neurovascular function in the relative absence of hyaluronan.

ECM and synapse status are linked in the aging mesolimbic dopamine system

Leveraging weighted gene correlation network analysis (Langfelder and Horvath, 2008) and downstream pathway analysis (Metascape) revealed three protein modules (yellow, brown, tan; **Figure 3**) that were strongly associated with the status of HAPLNs and other proteoglycans. Protein expression patterns of these modules were related to brain region, providing complementary evidence for observed regional differences in ECM composition between the VTA and NAc in our histological examination (**Figure 1**). The majority of excitatory and inhibitory synapse proteins showed similar abundances in young adult and aged mice, suggesting that robust synapse loss is not a feature of healthy midbrain or striatal aging. Homer2 abundance, which was found to not change by late middle-age (18 months) in histological experiments (**Figure 1**), did show significant reductions in this dataset. This difference could be related to the older ages used for proteomic analysis (22-24 months), or may reflect changes in Homer2 abundance at the post-synaptic density of individual synapses that are detectable with quantitative proteomic approaches but not light microscopy.

A critical finding from this analysis was that the abundance of numerous excitatory and inhibitory synaptic proteins was aligned with similar modules as matrisome proteins, but not with modules that contain proteins of the complement cascade. Microglial synapse engulfment through complement tagging has been implicated in declining synapse integrity and microglial phagocytic removal of synapses in numerous developmental and disease contexts (Morgan, 2018; Schafer et al., 2012; Stevens et al., 2007; Wilton et al., 2023). The absence of significant correlations between synapse and complement protein abundances in healthy aged brains

supports the hypothesis that aberrant complement-dependent synapse regulation may specifically be associated with synapse pathology in the context of age-associated disease. Conversely, these results suggest that the local status of the ECM plays more prominent roles in determining synapse numbers in the healthy aged brain.

An important note regarding this proteomic dataset is that inflammatory factors associated with microglia (e.g. TNFα and IL-6) were not detected. This is likely due to the fractionation protocol used specifically to enrich ECM and synaptic proteins. Previous reports indicate that microglial production of such inflammatory factors increases with age in the mesolimbic dopamine system; however, these differences are small and were detected using high-sensitivity ELISA protocols (Moca et al., 2022), which may be more sensitive to such cytokines compared to the fractionation approach used here. Future experiments in which inflammatory cytokines and ECM proteins are detected within the same samples will illuminate potential roles that inflammatory signaling plays in modulation ECM and synapse status in the aging brain.

Regional microglial aging phenotypes coincide with regional changes in hyaluronan matrix architecture

Previous work has demonstrated that VTA and NAc microglia show prominent regional differences in multiple physiological and transcriptional properties, as well as in their response to healthy aging (De Biase et al., 2017; Moca et al., 2022). Microglia densities in the NAc are roughly 30 percent higher compared to the VTA in young adult mice and increases in microglial proliferation and inflammatory factor production are evident by early middle age specifically in the VTA (Moca et al., 2022). The present observation that VTA microglial densities correlate with hyaluronan matrix distribution patterns suggests that these microglial aging phenotypes are associated with increases in the abundance of the ubiquitous ECM scaffold hyaluronan. This finding aligns with biochemical assessments of aged mouse brains that also demonstrate

greater hyaluronan abundance with age (Sugitani et al., 2021) and increased gene-expression of hyaluronan synthase molecules in the cerebral cortex of aged nonhuman primates (Cargill et al., 2012).

Further research will be needed to determine if VTA microglia primarily impact the ECM, or whether these interactions are bidirectional. Microglia express numerous cell surface receptors such as integrins and similar proteins that can sense the ECM (Bennett et al., 2016; Milner, 2009; Milner and Campbell, 2002; Zhang et al., 2014) and they may use this information to regulate production of degradative enzymes that would impact ECM abundance and structure. Hence, decreases in microglia-hyaluronan contacts (**Figure 5H**) within the aging VTA may represent decreased microglial ability to sense the local matrix, resulting in less local degradation or engagement of other mechanisms to promote local hyaluronan accumulation.

On the other hand, microglia may use adhesive interactions with the ECM scaffold to remodel their processes and interact with neurons, synapses, and other glial cells around which ECM structures accumulate. In support of this hypothesis, VTA microglia in aged mice exhibit reduced morphological complexity relative to young adult mice (Moca et al., 2022), which may be a consequence of VTA microglia making fewer contacts with the hyaluronan matrix in aging mice (**Figure 5H**). Furthermore, hyaluronan can regulate the inflammatory profiles of immune cells by binding to and sequestering proinflammatory receptors such as CD44 and Toll-like receptors, which microglia also express (Austin et al., 2012; Avenoso et al., 2019; Campo et al., 2010; Peters and Sherman, 2020; Soria et al., 2020; Tavianatou et al., 2019). This raises the possibility that certain aspects of microglial aging phenotypes may emerge due to changes in ECM-to-microglia signaling via immune receptors.

Constitutive microglial ablation increases hyaluronan deposition in the VTA

Microglial ablation through constitutive deletions of the FIRE enhancer of the Csfr1 locus resulted in greater hyaluronan matrix deposition in the VTA of young-adult mice. This finding suggests that microglia have a net antagonistic effect on ECM deposition, which aligns with previous reports demonstrating increases in cortical perineuronal net densities following transient microglial depletions using the Csf1r inhibitor PLX5622 in a 5xFAD model of Alzheimer's Disease (Crapser et al., 2020). Therefore, in a pathological context the presence of microglia reduces ECM deposition patterns with age, which is a phenotype that has also been observed in the substantia nigra pars compacta of a mouse model of Parkinson's Disease (Soria et al., 2020). The present study suggests that a key differentiating feature between healthy and pathological brain aging states is that, despite the presence of microglia, mesolimbic ECM deposition increases rather than decreases in the absence of pathology. Whether healthy microglial aging phenotypes actively facilitate increases in ECM abundance or rather are simply not as degradative as disease-associated microglia is not clear. Microglia do, however, produce hyaluronadherin molecules like TSG-6 that crosslink hyaluronan fibrils and promote matrix stability (Coulson-Thomas et al., 2016; Li et al., 2018).

Microglial fractalkine signaling promotes hyaluronan deposition and restricts excitatory synapse numbers in the aging ventral tegmental area

Previous reports have linked CX3CL1/CX3CR1 signaling with synapse numbers and ECM proteoglycan abundance in cortical and hippocampal regions, (Bolós et al., 2018), as well as ECM composition in a variety of tissues throughout the body (Rivas-Fuentes et al., 2020; Song et al., 2013). A critical finding from this study was that unlike wild-type mice that exhibited greater hyaluronan deposition with age, aging mice with a single copy of the Cx3Cr1 allele ($Cx3Cr1^{EGFP/+}$) showed less hyaluronan matrix abundance, and Cx3Cr1-knockout mice ($Cx3Cr1^{EGFP/EGFP}$) showed lower levels still. One consequence of these changes was that VTA microglia from Cx3Cr1-het mice made fewer contacts with the hyaluronan matrix with advanced

age (**Figure 5H**). Isolated Cx3Cr1-knockout microglia from young adult mice express elevated levels of inflammatory factors such as *Tnf* and *Il6* and exhibit transcriptional patterns that more closely match aging microglia from Cx3Cr1-sufficient mice compared to microglia from age-matched controls (Gyoneva et al., 2019). Furthermore, Cx3Cr1-het mice exhibit accelerated VTA microglial aging phenotypes characterized by increases in proliferation, inflammatory factor production, and lysosome swelling earlier in the lifespan (~13 months) compared to wild-type mice in which these changes are evident later in life (~18 months; Moca et al., 2022). The observation that accelerated microglial aging phenotypes in Cx3Cr1-het and Cx3Cr1-knockout mice are associated with decreased hyaluronan matrix deposition raises the possibility that ECM glycosaminoglycans play roles in buffering VTA microglia from further increases in proliferation and inflammatory factor production in aging wild-type mice (Moca et al., 2022).

Cx3Cr1 knockout resulted in greater homer2 puncta densities by middle age in the VTA, suggesting that microglial fractalkine signaling help prevent excess synaptic drive in this region. Gene expression of the CX3CL1 ligand is enriched in neurons compared to other cell types, and CX3CL1/CX3CR1 signaling has been shown to regulate synapse function in numerous contexts through mechanisms of targeted synapse pruning and control of neuronal membrane excitability (Basilico et al., 2019; Gunner et al., 2019; Kim et al., 2020). Young mice deficient in CX3CL1/CX3CR1 signaling exhibit significant deficits in synapse elimination following whisker lesions, which is a manipulation known to attenuate neuronal activity in sensory cortex (Gunner et al., 2019). The present data extend these observations by showing that knockout of microglial Cx3Cr1 receptors may elicit similar deficits in synapse elimination in the aging brain. Additional research is needed to determine whether changes in hyaluronan matrix deposition are causally involved in this synapse phenotype.

Material and Methods

Mice

This study uses C57Bl6 wild-type mice, CX3CR1$^{EGFP/+}$ and CX3CR1$^{EGFP/EGFP}$ mice, and Csf1r$^{+/+}$ and Csf1r$^{\Delta FIRE/\Delta FIRE}$ mice (Rojo et al., 2019). C57Bl6 wild-type mice were purchased from the National Institutes on Aging (NIA) colony (Bethesda, Maryland) or Jackson Laboratory (Bar Harbor, ME; stock #000664). CX3CR1$^{EGFP/EGFP}$ breeders on a C57Bl6 background were originally purchased from the Jackson Laboratory (stock #005582) and crossed with C57Bl6 wild-type mice to obtain heterozygous (CX3CR1$^{EGFP/+}$) mice and CX3CR1$^{EGFP/EGFP}$ mice to obtain homozygous mice (CX3CR1$^{EGFP/EGFP}$). In these mice, EGFP is knocked into the fractalkine receptor (CX3CR1) locus, which is a receptor expressed specifically by most myeloid-lineage cells, including microglia (Haskell et al., 2001; Jung et al., 2000). Previous work has demonstrated that EGFP expression in these mice is specific to microglial cells in the basal ganglia (De Biase et al., 2017). Csf1r$^{\Delta FIRE/\Delta FIRE}$ breeders on a B6CBAF1/J background were originally purchased from Jackson Laboratory (stock # 032783) and crossed with C57BL/6 mice after which their offspring were interbred. These mice carry CRISPR/Cas9 generated deletion of the fms-intronic regulatory element (FIRE) of the Csf1r gene (Rojo et al., 2019).

For immunohistochemical and histochemical experiments in wild-type mice, a total 12 young-adult (4 months; 6 male, 6 female) and 12 late-middle aged mice (18 months; 6 male, 6 female) were used. Imaris reconstructions were performed on images obtained from 5 young adult (3-4 months; 3 female, 2 male), 5 middle-aged (13-18 months, 3 female, 2 male), and 6 aged (21-24 months, 4 female, 2 male) CX3CR1$^{EGFP/+}$ mice. Histochemical quantifications of synapse and hyaluronan abundance in Cx3Cr1-deficient and knockout mice utilized 4 young-adult Cx3Cr1$^{EGFP/+}$ (3-4 months; 2 male, 2 female), 4 young-adult Cx3Cr1$^{EGFP/EGFP}$ (3-4 months; 2 male, 2 female), 4 middle-aged Cx3Cr1$^{EGFP/+}$ (12-15 months; 2 male, 2 female), and 4 middle-aged Cx3Cr1$^{EGFP/EGFP}$ mice (12-15 months; 2 male, 2 female). Histological examinations

comparing microglia-deficient mice with controls utilized 3 young-adult Csf1r$^{\Delta FIRE/\Delta FIRE}$ mice (3-4 months, 2 females, 1 male) and 3 young-adult Csf1r$^{+/+}$ mice (3-4 months, 1 female, 2 males). Quantitative proteomic experiments included 4 young-adult (3-4 mo; 2 male, 2 female) and 4 aged (22-24 mo; 2 male, 2 female) wild-type mice. All mice within a given experiment were housed in the same vivarium with a normal light/dark cycle and were provided *ad libitum* access to food and water. Experiments adhered to protocols approved by the Animal Care and Use Committee and UCLA.

Transcardial perfusion, immunohistochemistry, and histochemistry

Mice were deeply anesthetized in a covered beaker containing isofluorane and perfused transcardially with 1M phosphate buffered saline (PBS; pH 7.4) followed by ice-cold 4% paraformaldehyde (PFA) in 1M PBS. All perfusions were performed between 8:00 am and 12:00 pm to minimize the contribution that circadian changes may have on ECM, synapse, and microglial properties (Hayashi et al., 2013). Brains were extracted immediately following perfusions and were allowed to post-fix for ~4 hours in 4% PFA and then stored in 1M PBS with 0.1% sodium azide until tissue sectioning.

Coronal brain sections were prepared using a vibratome in chilled 1M PBS solution and stored in 1M PBS with 0.1% sodium azide until histochemical labelling. Sections containing the ventral tegmental area (VTA) and nucleus accumbens (NAc) were selected using well-defined anatomical landmarks at 3 distinct anterior-posterior locations per mouse. Free-floating brain sections were briefly rinsed in 1M PBS (5 minutes) and then permeabilized and blocked in a solution of 1% bovine serum albumin (BSA) and 0.1% saponin for 1 hour. Sections were then incubated with a biotinylated HABP lectin (1:250; Sigma-Aldrich cat: 385911) in the 1% BSA and 0.1% saponin block solution overnight at 4°C with mild agitation. Sections were washed in 1M PBS (4x10 minutes) and then incubated with streptavidin-conjugated AlexaFluor-647 in the 1% BSA and 0.1% saponin block solution for 2 hours. The tissue underwent another 4x10

minute wash in 1M PBS, and then was blocked again in 5% normal donkey serum with no additional permeabilization agent for 1 hour and then was incubated overnight with mild agitation in a solution containing different combinations of goat anti-GFP (1:1000; Frontier Institute cat: GFP-go-Af1480), rabbit-anti-IBA1 (1:500; Wako cat: 019-19741), chicken anti-TH (1:500; Aves cat: TYH), rabbit anti-Homer2 (1:2000; Synaptic Systems cat: 160 003), and the biotinylated HABP lectin in 5% NDS solution. Sections were again washed in 1M PBS (4x10 minutes). Prior to secondary antibody incubation, all sections were treated with TrueBlack lipofuscin autofluorescence quencher (5%; Biotium cat: 23007) for 90 seconds followed by a 3x5 minute rinse in 1M PBS. Sections were then incubated in a secondary antibody solution containing combinations of chicken AlexaFluor-405 or chicken AlexaFluor-594, goat AlexaFluor-488, rabbit AlexaFluor-488 or rabbit AlexaFluor594, and streptavidin-conjugated AlexaFluor-647 in 5% NDS for 2 hours at room temperature with mild agitation. The sections were again washed in 1M PBS (4x10 minutes) and were then mounted and coverslipped with coverslips of #1.5 thickness using Aqua-Poly/Mount (Polysciences cat: 18606).

Image acquisition and analysis

Fixed-tissue was imaged using a Zeiss LSM-700 confocal microscope using a 63x objective at a z interval of 0.3 μm or a Leica STELLARIS 5 confocal microscope using 20x (z = 1.5) and 63x objectives (z = 0.3). For quantification of hyaluronan fibril deposition patterns, 63x images were imported into Fiji image analysis software and underwent a background subtraction (rolling-ball radius = 5) and de-speckling. The processed images were then binarized using the 'MaxEntropy' setting and hyaluronan fibril densities and sizes were assessed using the 3D Object Counter plugin in Fiji using a minimum pixel cutoff of 10. Hyaluronan distribution regularity was quantified in the same images using the Fractal Dimension plugin in Fiji. Homer2 and putative hyaluronan-Homer2 densities were examined using the Analyze Puncta plugin in Fiji using stock setting as described previously in (Han et al.,

2022). Every 3 z-planes of the confocal stacks were z-projected (max intensity) and underwent analysis using this plugin.

Spatial correlations between microglia and hyaluronan were analyzed using 20x confocal stacks of histochemically labelled Cx3Cr1$^{EGFP/+}$ tissue. To obtain field-of-view correlations, hyaluronan and GFP channels were binarized after thresholding in Fiji and the proportion of hyaluronan and GFP pixels above threshold within each image was correlated. Microglia densities were calculated by manually counting microglial cell bodies within a z-stack using the Cell Counter plugin and then normalizing these counts by the volume of the image. More local measures of microglia-hyaluronan spatial correlations were assessed by overlaying a 10x10 grid over threshold 20x images using custom-written Fiji macros and the Pearson Correlation Coefficient of hyaluronan and microglial signal was calculated for each image using all 100 boxes of this grid.

Manual reconstructions of microglia and the hyaluronan matrix were done by importing high-magnification (63x) confocal z-stack images into Imaris (Bitplane; Belfast, UK) software for reconstruction using the surfaces module. For each channel, a threshold that most accurately represented the signal was manually set and surfaces smaller than 1 μm^3 were filtered out. Hyaluronan-microglia and hyaluronan-dopamine neuron contacts were captured by filtering the hyaluronan surface using the GFP or TH fluorescence histograms. The number of GFP/TH-filtered hyaluronan aggregates was normalized by the total GFP or TH signal within the field of view.

Quantitative proteomics: sample preparation

Young and aged wild-type mice were anesthetized with isofluorane and perfused with 1M PBS. Brains were extracted and the midbrain and striatum were dissected using a scalpel, minced, triturated, washed in 1M PBS, and stored at -80°C until further processing. Tissue was

processed using protocols from Naba et al., 2015 using a compartment protein extraction kit (Millipore cat: 2145). Triturated brain tissue was thawed on ice for ~30 minutes before being homogenized in 2 ml/g of Buffer C (HEPES (pH7.9), MgCl2, KCl, EDTA, Sucrose, Glycerol, Sodium OrthoVanadate) with protease inhibitors. This mixture was rotated on ice for 20 minutes and then spun at 20,000g at 4ºC for 20 minutes. The supernatant was removed and stored at -80ºC until proteomic analysis. The pellet was washed in 4 ml/g of the same buffer (HEPES (pH7.9), MgCl2, KCl, EDTA, Sucrose, Glycerol, Sodium OrthoVanadate) with protease inhibitors, rotated for 5 minutes at 4ºC, and spun at 20,000g at 4ºC for 20 minutes. The supernatant was removed and discarded. The pellet was then incubated in 1ml/g of Buffer N (HEPES (pH7.9), MgCl2, NAcl, EDTA, Glycerol, Sodium OrthoVanadate), rotated at 4ºC for 20 minutes, spun at 20,000g for 20 minutes, and the supernatant was removed and stored at -80ºC until proteomic analysis. The pellet was then washed in 1ml/g of Buffer M (HEPES (pH7.9), MgCl2, KCl, EDTA, Sucrose, Glycerol, Sodium deoxycholate, NP-40, Sodium OrthoVanadate), rotated at 4ºC for 20 minutes, spun at 20,000g for 20 minutes, and the supernatant was removed and stored at -80ºC until proteomic analysis. The pellet was washed in 0.5 ml/g of buffer CS (Pipes (pH6.8), MgCl2, NAcl, EDTA, Sucrose, SDS, Sodium OrthoVanadate), rotated at 4ºC for 20 minutes, spun at 20,000g for 20 minutes, and the supernatant was removed and stored at -80ºC until proteomic analysis. The final remaining insoluble pellet was also stored at -80ºC for proteomic analysis.

Samples were resuspended in equal volume of 8M Urea, 100mM Tris-Cl, pH. This was followed by reduction with TCEP and alkylation with IAA, followed by protein clean up with SP3 beads. Overnight digestion was done with trypsin and lysC enzymes. The peptides were cleaned using the SP3 protocol (Hughes et al., 2019), followed by elution in 2% DMSO. Samples were dried using a speed vacuum, and the dried peptides were resuspended in 5%

formic acid before being sent for liquid chromatotography with tandem mass spectrometry (LC-MS/MS).

Quantitative proteomics: analysis

MaxQuant software was used for peptide identification (Cox and Mann, 2008). These algorithms use correlational analyses and graph theory to measure multiple mass measurements, and then integrate across these measurements and corrects for linear and nonlinear mass offsets. Raw intensity data from each sample was batch corrected using a quantile normalization followed by a median centering procedure using the ComBat function in R. This procedure uses an iterative algorithm to find the point that minimizes Euclidean distance to all features in the dataset and adjusts the distribution from each batch to this point. The intensity data of each identified protein was then summed across solubility fractions for each mouse and was then log2 normalized for analysis. To be included in the analysis, a protein needed to be detected in 75% or more of the samples within a brain region. Fold changes were calculated as the ratio of the aged signal relative to the young signal. Statistical significance was assessed using unpaired t-tests with an alpha-level of 0.05. Annotations for different protein classes were downloaded from publicly available online databases. ECM protein annotations were downloaded from the Matrisome project database (Shao et al., 2023), innate immune system protein annotations from the InnateDB database (Lynn et al., 2008), and synapse protein annotations from the SynGo database (Koopmans et al., 2019).

Quantitative proteomics: weighted gene correlation network analysis (WGCNA)

To examine relationships between synaptic, matrisome, and innate immune proteins, proteomic data underwent unsupervised clustering using Weighted Gene Correlation Network Analysis (WGCNA) in R (Langfelder and Horvath, 2008). Processed log2(intensity) data from the midbrain and striatum were used for network construction. One striatal sample from an aged

female mouse was identified as an outlier and was removed from this analysis. WGCNA provides modules of covarying proteins that are agnostic to traits of the samples (i.e., age, region, sex). The distribution of synaptic, matrisome, and immune proteins across the protein modules was used to identify modules of interest for further analysis. Relationships between modules and external traits or protein abundance were examined using the module-trait relationship code provided in the WGCNA R package. Process enrichment analysis of the protein modules was conducted in Metascape (Zhou et al., 2019) using default parameters.

References

Austin, J.W., Gilchrist, C., Fehlings, M.G., 2012. High molecular weight hyaluronan reduces lipopolysaccharide mediated microglial activation. Journal of Neurochemistry 122, 344–355. https://doi.org/10.1111/j.1471-4159.2012.07789.x

Avenoso, A., Bruschetta, G., D'Ascola, A., Scuruchi, M., Mandraffino, G., Gullace, R., Saitta, A., Campo, S., Campo, G.M., 2019. Hyaluronan fragments produced during tissue injury: A signal amplifying the inflammatory response. Archives of Biochemistry and Biophysics 663, 228–238. https://doi.org/10.1016/j.abb.2019.01.015

Ayata, P., Badimon, A., Strasburger, H.J., Duff, M.K., Montgomery, S.E., Loh, Y.-H.E., Ebert, A., Pimenova, A.A., Ramirez, B.R., Chan, A.T., Sullivan, J.M., Purushothaman, I., Scarpa, J.R., Goate, A.M., Busslinger, M., Shen, L., Losic, B., Schaefer, A., 2018. Epigenetic regulation of brain region-specific microglia clearance activity. Nat Neurosci 21, 1049–1060. https://doi.org/10.1038/s41593-018-0192-3

Bäckman, L., Lindenberger, U., Li, S.-C., Nyberg, L., 2010. Linking cognitive aging to alterations in dopamine neurotransmitter functioning: Recent data and future avenues. Neuroscience & Biobehavioral Reviews, Special Section: Dopaminergic Modulation of Lifespan Cognition 34, 670–677. https://doi.org/10.1016/j.neubiorev.2009.12.008

Bäckman, L., Nyberg, L., Lindenberger, U., Li, S.-C., Farde, L., 2006. The correlative triad among aging, dopamine, and cognition: Current status and future prospects. Neuroscience & Biobehavioral Reviews, Methodological and Conceptual Advances in the Study of Brain-Behavior Dynamics: A Multivariate Lifespan Perspective 30, 791–807. https://doi.org/10.1016/j.neubiorev.2006.06.005

Badimon, A., Strasburger, H.J., Ayata, P., Chen, X., Nair, A., Ikegami, A., Hwang, P., Chan, A.T., Graves, S.M., Uweru, J.O., Ledderose, C., Kutlu, M.G., Wheeler, M.A., Kahan, A., Ishikawa, M., Wang, Y.-C., Loh, Y.-H.E., Jiang, J.X., Surmeier, D.J., Robson, S.C., Junger, W.G., Sebra, R., Calipari, E.S., Kenny, P.J., Eyo, U.B., Colonna, M., Quintana, F.J., Wake, H., Gradinaru, V., Schaefer, A., 2020. Negative feedback control of neuronal activity by microglia. Nature 586, 417–423. https://doi.org/10.1038/s41586-020-2777-8

Baig, S., Wilcock, G.K., Love, S., 2005. Loss of perineuronal net N-acetylgalactosamine in Alzheimer's disease. Acta Neuropathol 110, 393–401. https://doi.org/10.1007/s00401-005-1060-2

Banks, W.A., Reed, M.J., Logsdon, A.F., Rhea, E.M., Erickson, M.A., 2021. Healthy aging and the blood-brain barrier. Nat Aging 1, 243–254. https://doi.org/10.1038/s43587-021-00043-5

Barnes, C.A., 1979. Memory deficits associated with senescence: a neurophysiological and behavioral study in the rat. J Comp Physiol Psychol 93, 74–104. https://doi.org/10.1037/h0077579

Basilico, B., Pagani, F., Grimaldi, A., Cortese, B., Di Angelantonio, S., Weinhard, L., Gross, C., Limatola, C., Maggi, L., Ragozzino, D., 2019. Microglia shape presynaptic properties at developing glutamatergic synapses. Glia 67, 53–67. https://doi.org/10.1002/glia.23508

Bennett, M.L., Bennett, F.C., Liddelow, S.A., Ajami, B., Zamanian, J.L., Fernhoff, N.B., Mulinyawe, S.B., Bohlen, C.J., Adil, A., Tucker, A., Weissman, I.L., Chang, E.F., Li, G., Grant, G.A., Gephart, M.G.H., Barres, B.A., 2016. New tools for studying microglia in the mouse and human CNS. PNAS 113, E1738–E1746. https://doi.org/10.1073/pnas.1525528113

Berry, A.S., Shah, V.D., Baker, S.L., Vogel, J.W., O'Neil, J.P., Janabi, M., Schwimmer, H.D., Marks, S.M., Jagust, W.J., 2016. Aging Affects Dopaminergic Neural Mechanisms of Cognitive Flexibility. J. Neurosci. 36, 12559–12569. https://doi.org/10.1523/JNEUROSCI.0626-16.2016

Bolós, M., Perea, J.R., Terreros-Roncal, J., Pallas-Bazarra, N., Jurado-Arjona, J., Ávila, J., Llorens-Martín, M., 2018. Absence of microglial CX3CR1 impairs the synaptic integration of adult-born

hippocampal granule neurons. Brain, Behavior, and Immunity 68, 76–89. https://doi.org/10.1016/j.bbi.2017.10.002

Brückner, G., Brauer, K., Härtig, W., Wolff, J.R., Rickmann, M.J., Derouiche, A., Delpech, B., Girard, N., Oertel, W.H., Reichenbach, A., 1993. Perineuronal nets provide a polyanionic, glia-associated form of microenvironment around certain neurons in many parts of the rat brain. Glia 8, 183–200. https://doi.org/10.1002/glia.440080306

Brückner, G., Hausen, D., Härtig, W., Drlicek, M., Arendt, T., Brauer, K., 1999. Cortical areas abundant in extracellular matrix chondroitin sulphate proteoglycans are less affected by cytoskeletal changes in Alzheimer's disease. Neuroscience 92, 791–805. https://doi.org/10.1016/S0306-4522(99)00071-8

Burke, S.N., Barnes, C.A., 2006. Neural plasticity in the ageing brain. Nat Rev Neurosci 7, 30–40. https://doi.org/10.1038/nrn1809

Campo, G.M., Avenoso, A., Campo, S., D'Ascola, A., Nastasi, G., Calatroni, A., 2010. Small hyaluronan oligosaccharides induce inflammation by engaging both toll-like-4 and CD44 receptors in human chondrocytes. Biochemical Pharmacology 80, 480–490. https://doi.org/10.1016/j.bcp.2010.04.024

Cargill, R., Kohama, S.G., Struve, J., Su, W., Banine, F., Witkowski, E., Back, S.A., Sherman, L.S., 2012. Astrocytes in aged non-human primate brain gray matter synthesize excess hyaluronan. Neurobiol Aging 33, 830.e13-830.e24. https://doi.org/10.1016/j.neurobiolaging.2011.07.006

Chang, M.C., Park, J.M., Pelkey, K.A., Grabenstatter, H.L., Xu, D., Linden, D.J., Sutula, T.P., McBain, C.J., Worley, P.F., 2010. Narp regulates homeostatic scaling of excitatory synapses on parvalbumin-expressing interneurons. Nat Neurosci 13, 1090–1097. https://doi.org/10.1038/nn.2621

Chiquet-Ehrismann, R., 2004. Tenascins. The International Journal of Biochemistry & Cell Biology, Modulatory Adhesion Molecules in Tissue Homeostasis 36, 986–990. https://doi.org/10.1016/j.biocel.2003.12.002

Coulson-Thomas, V.J., Lauer, M.E., Soleman, S., Zhao, C., Hascall, V.C., Day, A.J., Fawcett, J.W., 2016. Tumor Necrosis Factor-stimulated Gene-6 (TSG-6) Is Constitutively Expressed in Adult Central Nervous System (CNS) and Associated with Astrocyte-mediated Glial Scar Formation following Spinal Cord Injury. J Biol Chem 291, 19939–19952. https://doi.org/10.1074/jbc.M115.710673

Cox, J., Mann, M., 2008. MaxQuant enables high peptide identification rates, individualized p.p.b.-range mass accuracies and proteome-wide protein quantification. Nat Biotechnol 26, 1367–1372. https://doi.org/10.1038/nbt.1511

Crapser, J.D., Arreola, M.A., Tsourmas, K.I., Green, K.N., 2021. Microglia as hackers of the matrix: sculpting synapses and the extracellular space. Cell Mol Immunol 18, 2472–2488. https://doi.org/10.1038/s41423-021-00751-3

Crapser, J.D., Spangenberg, E.E., Barahona, R.A., Arreola, M.A., Hohsfield, L.A., Green, K.N., 2020. Microglia facilitate loss of perineuronal nets in the Alzheimer's disease brain. EBioMedicine 58, 102919. https://doi.org/10.1016/j.ebiom.2020.102919

Cserép, C., Pósfai, B., Lénárt, N., Fekete, R., László, Z.I., Lele, Z., Orsolits, B., Molnár, G., Heindl, S., Schwarcz, A.D., Ujvári, K., Környei, Z., Tóth, K., Szabadits, E., Sperlágh, B., Baranyi, M., Csiba, L., Hortobágyi, T., Maglóczky, Z., Martinecz, B., Szabó, G., Erdélyi, F., Szipőcs, R., Tamkun, M.M., Gesierich, B., Duering, M., Katona, I., Liesz, A., Tamás, G., Dénes, Á., 2020. Microglia monitor and protect neuronal function through specialized somatic purinergic junctions. Science. https://doi.org/10.1126/science.aax6752

Dahl, M.J., Bachman, S.L., Dutt, S., Düzel, S., Bodammer, N.C., Lindenberger, U., Kühn, S., Werkle-Bergner, M., Mather, M., 2023. The integrity of dopaminergic and noradrenergic brain regions is associated with different aspects of late-life memory performance. Nat Aging 3, 1128–1143. https://doi.org/10.1038/s43587-023-00469-z

Dauth, S., Grevesse, T., Pantazopoulos, H., Campbell, P.H., Maoz, B.M., Berretta, S., Parker, K.K., 2016. Extracellular matrix protein expression is brain region dependent. Journal of Comparative Neurology 524, 1309–1336. https://doi.org/10.1002/cne.23965

De Biase, L.M., Schuebel, K.E., Fusfeld, Z.H., Jair, K., Hawes, I.A., Cimbro, R., Zhang, H.-Y., Liu, Q.-R., Shen, H., Xi, Z.-X., Goldman, D., Bonci, A., 2017. Local Cues Establish and Maintain Region-Specific Phenotypes of Basal Ganglia Microglia. Neuron 95, 341-356.e6. https://doi.org/10.1016/j.neuron.2017.06.020

Dityatev, A., Schachner, M., Sonderegger, P., 2010. The dual role of the extracellular matrix in synaptic plasticity and homeostasis. Nat Rev Neurosci 11, 735–746. https://doi.org/10.1038/nrn2898

Dumitriu, D., Hao, J., Hara, Y., Kaufmann, J., Janssen, W.G.M., Lou, W., Rapp, P.R., Morrison, J.H., 2010. Selective Changes in Thin Spine Density and Morphology in Monkey Prefrontal Cortex Correlate with Aging-Related Cognitive Impairment. J. Neurosci. 30, 7507–7515. https://doi.org/10.1523/JNEUROSCI.6410-09.2010

Evers, M.R., Salmen, B., Bukalo, O., Rollenhagen, A., Bösl, M.R., Morellini, F., Bartsch, U., Dityatev, A., Schachner, M., 2002. Impairment of L-type Ca2+ Channel-Dependent Forms of Hippocampal Synaptic Plasticity in Mice Deficient in the Extracellular Matrix Glycoprotein Tenascin-C. J. Neurosci. 22, 7177–7194. https://doi.org/10.1523/JNEUROSCI.22-16-07177.2002

Fawcett, J.W., Kwok, J.C.F., 2022. Proteoglycan Sulphation in the Function of the Mature Central Nervous System. Frontiers in Integrative Neuroscience 16.

Felsky, D., Patrick, E., Schneider, J.A., Mostafavi, S., Gaiteri, C., Patsopoulos, N., Bennett, D.A., De Jager, P.L., 2018. Polygenic analysis of inflammatory disease variants and effects on microglia in the aging brain. Mol Neurodegeneration 13, 38. https://doi.org/10.1186/s13024-018-0272-6

Felsky, D., Roostaei, T., Nho, K., Risacher, S.L., Bradshaw, E.M., Petyuk, V., Schneider, J.A., Saykin, A., Bennett, D.A., De Jager, P.L., 2019. Neuropathological correlates and genetic architecture of microglial activation in elderly human brain. Nat Commun 10, 409. https://doi.org/10.1038/s41467-018-08279-3

Foscarin, S., Raha-Chowdhury, R., Fawcett, J.W., Kwok, J.C.F., 2017. Brain ageing changes proteoglycan sulfation, rendering perineuronal nets more inhibitory. Aging (Albany NY) 9, 1607–1622. https://doi.org/10.18632/aging.101256

Frischknecht, R., Gundelfinger, E.D., 2012. The Brain's Extracellular Matrix and Its Role in Synaptic Plasticity, in: Kreutz, M.R., Sala, C. (Eds.), Synaptic Plasticity: Dynamics, Development and Disease, Advances in Experimental Medicine and Biology. Springer, Vienna, pp. 153–171. https://doi.org/10.1007/978-3-7091-0932-8_7

Frischknecht, R., Heine, M., Perrais, D., Seidenbecher, C.I., Choquet, D., Gundelfinger, E.D., 2009. Brain extracellular matrix affects AMPA receptor lateral mobility and short-term synaptic plasticity. Nat Neurosci 12, 897–904. https://doi.org/10.1038/nn.2338

Grabert, K., Michoel, T., Karavolos, M.H., Clohisey, S., Baillie, J.K., Stevens, M.P., Freeman, T.C., Summers, K.M., McColl, B.W., 2016. Microglial brain region−dependent diversity and selective regional sensitivities to aging. Nature Neuroscience 19, 504–516. https://doi.org/10.1038/nn.4222

Gray, D.T., Khattab, S., Meltzer, J., McDermott, K., Schwyhart, R., Sinakevitch, I., Härtig, W., Barnes, C.A., 2022. Retrosplenial cortex microglia and perineuronal net densities are associated with memory impairment in aged rhesus macaques. Cerebral Cortex bhac366. https://doi.org/10.1093/cercor/bhac366

Gray, D.T., Zempare, M., Carey, N., Khattab, S., Sinakevitch, I., De Biase, L.M., Barnes, C.A., 2023. Extracellular matrix proteoglycans support aged hippocampus networks: a potential cellular-level mechanism of brain reserve. Neurobiology of Aging 131, 52–58. https://doi.org/10.1016/j.neurobiolaging.2023.07.010

Gunner, G., Cheadle, L., Johnson, K.M., Ayata, P., Badimon, A., Mondo, E., Nagy, M.A., Liu, L., Bemiller, S.M., Kim, K.-W., Lira, S.A., Lamb, B.T., Tapper, A.R., Ransohoff, R.M., Greenberg, M.E., Schaefer, A., Schafer, D.P., 2019. Sensory lesioning induces microglial synapse elimination via ADAM10 and fractalkine signaling. Nat Neurosci 22, 1075–1088. https://doi.org/10.1038/s41593-019-0419-y

Gyoneva, S., Hosur, R., Gosselin, D., Zhang, B., Ouyang, Z., Cotleur, A.C., Peterson, M., Allaire, N., Challa, R., Cullen, P., Roberts, C., Miao, K., Reynolds, T.L., Glass, C.K., Burkly, L., Ransohoff, R.M., 2019. Cx3cr1-deficient microglia exhibit a premature aging transcriptome. Life Sci Alliance 2, e201900453. https://doi.org/10.26508/lsa.201900453

Haberman, R.P., Koh, M.T., Gallagher, M., 2017. Heightened cortical excitability in aged rodents with memory impairment. Neurobiology of Aging 54, 144–151. https://doi.org/10.1016/j.neurobiolaging.2016.12.021

Hamill, K.J., Kligys, K., Hopkinson, S.B., Jones, J.C.R., 2009. Laminin deposition in the extracellular matrix: a complex picture emerges. Journal of Cell Science 122, 4409–4417. https://doi.org/10.1242/jcs.041095

Han, R.T., Vainchtein, I.D., Schlachetzki, J.C.M., Cho, F.S., Dorman, L.C., Ahn, E., Kim, D.K., Barron, J.J., Nakao-Inoue, H., Molofsky, A.B., Glass, C.K., Paz, J.T., Molofsky, A.V., 2022. Microglial pattern recognition via IL-33 promotes synaptic refinement in developing corticothalamic circuits in mice. Journal of Experimental Medicine 220, e20220605. https://doi.org/10.1084/jem.20220605

Hara, Y., Rapp, P.R., Morrison, J.H., 2012. Neuronal and morphological bases of cognitive decline in aged rhesus monkeys. Age (Dordr) 34, 1051–1073. https://doi.org/10.1007/s11357-011-9278-5

Härtig, W., Brauer, K., Brückner, G., 1992. Wisteria floribunda agglutinin-labelled nets surround parvalbumin-containing neurons. Neuroreport 3, 869–872. https://doi.org/10.1097/00001756-199210000-00012

Haskell, C.A., Hancock, W.W., Salant, D.J., Gao, W., Csizmadia, V., Peters, W., Faia, K., Fituri, O., Rottman, J.B., Charo, I.F., 2001. Targeted deletion of CX(3)CR1 reveals a role for fractalkine in cardiac allograft rejection. J Clin Invest 108, 679–688. https://doi.org/10.1172/JCI12976

Hayashi, Y., Koyanagi, S., Kusunose, N., Okada, R., Wu, Z., Tozaki-Saitoh, H., Ukai, K., Kohsaka, S., Inoue, K., Ohdo, S., Nakanishi, H., 2013. The intrinsic microglial molecular clock controls synaptic strength via the circadian expression of cathepsin S. Sci Rep 3, 2744. https://doi.org/10.1038/srep02744

Hirakawa, S., Oohashi, T., Su, W.-D., Yoshioka, H., Murakami, T., Arata, J., Ninomiya, Y., 2000. The Brain Link Protein-1 (BRAL1): cDNA Cloning, Genomic Structure, and Characterization as a Novel Link Protein Expressed in Adult Brain. Biochemical and Biophysical Research Communications 276, 982–989. https://doi.org/10.1006/bbrc.2000.3583

Hobohm, C., Härtig, W., Brauer, K., Brückner, G., 1998. Low expression of extracellular matrix components in rat brain stem regions containing modulatory aminergic neurons. Journal of Chemical Neuroanatomy 15, 135–142. https://doi.org/10.1016/S0891-0618(98)00044-1

Hope, K.T., Hawes, I.A., Moca, E.N., Bonci, A., De Biase, L.M., 2020. Maturation of the microglial population varies across mesolimbic nuclei. European Journal of Neuroscience 52, 3689–3709. https://doi.org/10.1111/ejn.14740

Hu, J., Chen, Q., Zhu, H., Hou, L., Liu, W., Yang, Q., Shen, H., Chai, G., Zhang, B., Chen, Shaoxuan, Cai, Z., Wu, C., Hong, F., Li, H., Chen, Sifang, Xiao, N., Wang, Z., Zhang, X., Wang, B., Zhang, L., Mo, W., 2023. Microglial Piezo1 senses Aβ fibril stiffness to restrict Alzheimer's disease. Neuron 111, 15-29.e8. https://doi.org/10.1016/j.neuron.2022.10.021

Hughes, C.S., Moggridge, S., Müller, T., Sorensen, P.H., Morin, G.B., Krijgsveld, J., 2019. Single-pot, solid-phase-enhanced sample preparation for proteomics experiments. Nat Protoc 14, 68–85. https://doi.org/10.1038/s41596-018-0082-x

Iorio, V., Troughton, L.D., Hamill, K.J., 2015. Laminins: Roles and Utility in Wound Repair. Adv Wound Care (New Rochelle) 4, 250–263. https://doi.org/10.1089/wound.2014.0533

Jung, S., Aliberti, J., Graemmel, P., Sunshine, M.J., Kreutzberg, G.W., Sher, A., Littman, D.R., 2000. Analysis of fractalkine receptor CX(3)CR1 function by targeted deletion and green fluorescent protein reporter gene insertion. Mol Cell Biol 20, 4106–4114. https://doi.org/10.1128/MCB.20.11.4106-4114.2000

Kaczorowski, C.C., Disterhoft, J.F., 2009. Memory deficits are associated with impaired ability to modulate neuronal excitability in middle-aged mice. Learn Mem 16, 362–366. https://doi.org/10.1101/lm.1365609

Kim, A., García-García, E., Straccia, M., Comella-Bolla, A., Miguez, A., Masana, M., Alberch, J., Canals, J.M., Rodríguez, M.J., 2020. Reduced Fractalkine Levels Lead to Striatal Synaptic Plasticity Deficits in Huntington's Disease. Front Cell Neurosci 14, 163. https://doi.org/10.3389/fncel.2020.00163

Klein, S.L., Flanagan, K.L., 2016. Sex differences in immune responses. Nat Rev Immunol 16, 626–638. https://doi.org/10.1038/nri.2016.90

Koopmans, F., van Nierop, P., Andres-Alonso, M., Byrnes, A., Cijsouw, T., Coba, M.P., Cornelisse, L.N., Farrell, R.J., Goldschmidt, H.L., Howrigan, D.P., Hussain, N.K., Imig, C., de Jong, A.P.H., Jung, H., Kohansalnodehi, M., Kramarz, B., Lipstein, N., Lovering, R.C., MacGillavry, H., Mariano, V., Mi, H., Ninov, M., Osumi-Sutherland, D., Pielot, R., Smalla, K.-H., Tang, H., Tashman, K., Toonen, R.F.G., Verpelli, C., Reig-Viader, R., Watanabe, K., van Weering, J., Achsel, T., Ashrafi, G., Asi, N., Brown, T.C., De Camilli, P., Feuermann, M., Foulger, R.E., Gaudet, P., Joglekar, A., Kanellopoulos, A., Malenka, R., Nicoll, R.A., Pulido, C., de Juan-Sanz, J., Sheng, M., Südhof, T.C., Tilgner, H.U., Bagni, C., Bayés, À., Biederer, T., Brose, N., Chua, J.J.E., Dieterich, D.C., Gundelfinger, E.D., Hoogenraad, C., Huganir, R.L., Jahn, R., Kaeser, P.S., Kim, E., Kreutz, M.R., McPherson, P.S., Neale, B.M., O'Connor, V., Posthuma, D., Ryan, T.A., Sala, C., Feng, G., Hyman, S.E., Thomas, P.D., Smit, A.B., Verhage, M., 2019. SynGO: An Evidence-Based, Expert-Curated Knowledge Base for the Synapse. Neuron 103, 217-234.e4. https://doi.org/10.1016/j.neuron.2019.05.002

Kuo, D.S., Labelle-Dumais, C., Gould, D.B., 2012. COL4A1 and COL4A2 mutations and disease: insights into pathogenic mechanisms and potential therapeutic targets. Hum Mol Genet 21, R97–R110. https://doi.org/10.1093/hmg/dds346

Langfelder, P., Horvath, S., 2008. WGCNA: an R package for weighted correlation network analysis. BMC Bioinformatics 9, 559. https://doi.org/10.1186/1471-2105-9-559

Lensjø, K.K., Christensen, A.C., Tennøe, S., Fyhn, M., Hafting, T., 2017. Differential Expression and Cell-Type Specificity of Perineuronal Nets in Hippocampus, Medial Entorhinal Cortex, and Visual Cortex Examined in the Rat and Mouse. eNeuro 4. https://doi.org/10.1523/ENEURO.0379-16.2017

Lewitus, G.M., Konefal, S.C., Greenhalgh, A.D., Pribiag, H., Augereau, K., Stellwagen, D., 2016. Microglial TNF-α Suppresses Cocaine-Induced Plasticity and Behavioral Sensitization. Neuron 90, 483–491. https://doi.org/10.1016/j.neuron.2016.03.030

Li, R., Liu, W., Yin, J., Chen, Y., Guo, S., Fan, H., Li, X., Zhang, X., He, X., Duan, C., 2018. TSG-6 attenuates inflammation-induced brain injury via modulation of microglial polarization in SAH rats through the SOCS3/STAT3 pathway. Journal of Neuroinflammation 15, 231. https://doi.org/10.1186/s12974-018-1279-1

Long, K.R., Newland, B., Florio, M., Kalebic, N., Langen, B., Kolterer, A., Wimberger, P., Huttner, W.B., 2018. Extracellular Matrix Components HAPLN1, Lumican, and Collagen I Cause Hyaluronic Acid-Dependent Folding of the Developing Human Neocortex. Neuron 99, 702-719.e6. https://doi.org/10.1016/j.neuron.2018.07.013

Lynn, D.J., Winsor, G.L., Chan, C., Richard, N., Laird, M.R., Barsky, A., Gardy, J.L., Roche, F.M., Chan, T.H.W., Shah, N., Lo, R., Naseer, M., Que, J., Yau, M., Acab, M., Tulpan, D., Whiteside, M.D., Chikatamarla, A., Mah, B., Munzner, T., Hokamp, K., Hancock, R.E.W., Brinkman, F.S.L., 2008. InnateDB: facilitating systems-level analyses of the mammalian innate immune response. Molecular Systems Biology 4, 218. https://doi.org/10.1038/msb.2008.55

Mangold, C.A., Wronowski, B., Du, M., Masser, D.R., Hadad, N., Bixler, G.V., Brucklacher, R.M., Ford, M.M., Sonntag, W.E., Freeman, W.M., 2017. Sexually divergent induction of microglial-associated neuroinflammation with hippocampal aging. J Neuroinflammation 14, 141. https://doi.org/10.1186/s12974-017-0920-8

Midwood, K.S., Schwarzbauer, J.E., 2002. Tenascin-C Modulates Matrix Contraction via Focal Adhesion Kinase– and Rho-mediated Signaling Pathways. MBoC 13, 3601–3613. https://doi.org/10.1091/mbc.e02-05-0292

Milner, R., 2009. Microglial expression of αvβ3 and αvβ5 integrins is regulated by cytokines and the extracellular matrix: β5 Integrin null microglia show no defects in adhesion or MMP-9 expression on vitronectin. Glia 57, 714–723. https://doi.org/10.1002/glia.20799

Milner, R., Campbell, I.L., 2002. Cytokines Regulate Microglial Adhesion to Laminin and Astrocyte Extracellular Matrix via Protein Kinase C-Dependent Activation of the α6β1 Integrin. J. Neurosci. 22, 1562–1572. https://doi.org/10.1523/JNEUROSCI.22-05-01562.2002

Miroshnikova, Y.A., Mouw, J.K., Barnes, J.M., Pickup, M.W., Lakins, J.N., Kim, Y., Lobo, K., Persson, A.I., Reis, G.F., McKnight, T.R., Holland, E.C., Phillips, J.J., Weaver, V.M., 2016. Tissue mechanics promote IDH1-dependent HIF1α–tenascin C feedback to regulate glioblastoma aggression. Nat Cell Biol 18, 1336–1345. https://doi.org/10.1038/ncb3429

Miyamoto, A., Wake, H., Ishikawa, A.W., Eto, K., Shibata, K., Murakoshi, H., Koizumi, S., Moorhouse, A.J., Yoshimura, Y., Nabekura, J., 2016. Microglia contact induces synapse formation in developing somatosensory cortex. Nat Commun 7, 12540. https://doi.org/10.1038/ncomms12540

Moca, E.N., Lecca, D., Hope, K.T., Etienne, F., Schaler, A.W., Espinoza, K., Chappell, M.S., Gray, D.T., Tweedie, D., Sidhu, S., Masukawa, L., Sitoy, H., Mathew, R., Saban, D.R., Greig, N.H., Biase, L.M.D., 2022. Microglia Drive Pockets of Neuroinflammation in Middle Age. J. Neurosci. 42, 3896–3918. https://doi.org/10.1523/JNEUROSCI.1922-21.2022

Morgan, B.P., 2018. Complement in the pathogenesis of Alzheimer's disease. Semin Immunopathol 40, 113–124. https://doi.org/10.1007/s00281-017-0662-9

Morrison, J.H., Baxter, M.G., 2012. The ageing cortical synapse: hallmarks and implications for cognitive decline. Nat Rev Neurosci 13, 240–250. https://doi.org/10.1038/nrn3200

Mueller-Buehl, C., Reinhard, J., Roll, L., Bader, V., Winklhofer, K.F., Faissner, A., 2022. Brevican, Neurocan, Tenascin-C, and Tenascin-R Act as Important Regulators of the Interplay Between Perineuronal Nets, Synaptic Integrity, Inhibitory Interneurons, and Otx2. Frontiers in Cell and Developmental Biology 10.

Naba, A., Clauser, K.R., Hynes, R.O., 2015. Enrichment of Extracellular Matrix Proteins from Tissues and Digestion into Peptides for Mass Spectrometry Analysis. J Vis Exp 53057. https://doi.org/10.3791/53057

Neyazi, B., Stein, K.-P., Wilkens, L., Maslehaty, H., Dumitru, C.A., Sandalcioglu, I.E., 2020. Age-dependent changes of collagen alpha-2(IV) expression in the extracellular matrix of brain arteriovenous malformations. Clinical Neurology and Neurosurgery 189, 105589. https://doi.org/10.1016/j.clineuro.2019.105589

Nguyen, P.T., Dorman, L.C., Pan, S., Vainchtein, I.D., Han, R.T., Nakao-Inoue, H., Taloma, S.E., Barron, J.J., Molofsky, A.B., Kheirbek, M.A., Molofsky, A.V., 2020. Microglial Remodeling of the Extracellular Matrix Promotes Synapse Plasticity. Cell 182, 388-403.e15. https://doi.org/10.1016/j.cell.2020.05.050

Norris, C.M., Korol, D.L., Foster, T.C., 1996. Increased Susceptibility to Induction of Long-Term Depression and Long-Term Potentiation Reversal during Aging. J. Neurosci. 16, 5382–5392. https://doi.org/10.1523/JNEUROSCI.16-17-05382.1996

Oh, M.M., Oliveira, F.A., Disterhoft, J.F., 2010. Learning and Aging Related Changes in Intrinsic Neuronal Excitability. Front Aging Neurosci 2, 2. https://doi.org/10.3389/neuro.24.002.2010

Paolicelli, R.C., Bolasco, G., Pagani, F., Maggi, L., Scianni, M., Panzanelli, P., Giustetto, M., Ferreira, T.A., Guiducci, E., Dumas, L., Ragozzino, D., Gross, C.T., 2011. Synaptic Pruning by Microglia Is Necessary for Normal Brain Development. Science 333, 1456–1458. https://doi.org/10.1126/science.1202529

Parkhurst, C.N., Yang, G., Ninan, I., Savas, J.N., Yates, J.R., Lafaille, J.J., Hempstead, B.L., Littman, D.R., Gan, W.-B., 2013. Microglia promote learning-dependent synapse formation through brain-derived neurotrophic factor. Cell 155, 1596–1609. https://doi.org/10.1016/j.cell.2013.11.030

Perkins, K.L., Arranz, A.M., Yamaguchi, Y., Hrabetova, S., 2017. Brain extracellular space, hyaluronan, and the prevention of epileptic seizures. Rev Neurosci 28, 869–892. https://doi.org/10.1515/revneuro-2017-0017

Peters, A., Sherman, L.S., 2020. Diverse Roles for Hyaluronan and Hyaluronan Receptors in the Developing and Adult Nervous System. Int J Mol Sci 21, 5988. https://doi.org/10.3390/ijms21175988

Pizzorusso, T., Medini, P., Berardi, N., Chierzi, S., Fawcett, J.W., Maffei, L., 2002. Reactivation of Ocular Dominance Plasticity in the Adult Visual Cortex. Science. https://doi.org/10.1126/science.1072699

Pizzorusso, T., Medini, P., Landi, S., Baldini, S., Berardi, N., Maffei, L., 2006. Structural and functional recovery from early monocular deprivation in adult rats. Proc Natl Acad Sci U S A 103, 8517–8522. https://doi.org/10.1073/pnas.0602657103

Prater, K.E., Green, K.J., Mamde, S., Sun, W., Cochoit, A., Smith, C.L., Chiou, K.L., Heath, L., Rose, S.E., Wiley, J., Keene, C.D., Kwon, R.Y., Snyder-Mackler, N., Blue, E.E., Logsdon, B., Young, J.E., Shojaie, A., Garden, G.A., Jayadev, S., 2023. Human microglia show unique transcriptional changes in Alzheimer's disease. Nat Aging 3, 894–907. https://doi.org/10.1038/s43587-023-00424-y

Procès, A., Luciano, M., Kalukula, Y., Ris, L., Gabriele, S., 2022. Multiscale Mechanobiology in Brain Physiology and Diseases. Frontiers in Cell and Developmental Biology 10.

Reed, M.J., Damodarasamy, M., Pathan, J.L., Chan, C.K., Spiekerman, C., Wight, T.N., Banks, W.A., Day, A.J., Vernon, R.B., Keene, C.D., 2019. Increased Hyaluronan and TSG-6 in Association with Neuropathologic Changes of Alzheimer's Disease. Journal of Alzheimer's Disease 67, 91–102. https://doi.org/10.3233/JAD-180797

Reed, M.J., Vernon, R.B., Damodarasamy, M., Chan, C.K., Wight, T.N., Bentov, I., Banks, W.A., 2017. Microvasculature of the Mouse Cerebral Cortex Exhibits Increased Accumulation and Synthesis of Hyaluronan With Aging. J Gerontol A Biol Sci Med Sci 72, 740–746. https://doi.org/10.1093/gerona/glw213

Rivas-Fuentes, S., Herrera, I., Salgado-Aguayo, A., Buendía-Roldán, I., Becerril, C., Cisneros, J., 2020. CX3CL1 and CX3CR1 could be a relevant molecular axis in the pathophysiology of idiopathic pulmonary fibrosis. Int J Med Sci 17, 2357–2361. https://doi.org/10.7150/ijms.43748

Rojo, R., Raper, A., Ozdemir, D.D., Lefevre, L., Grabert, K., Wollscheid-Lengeling, E., Bradford, B., Caruso, M., Gazova, I., Sánchez, A., Lisowski, Z.M., Alves, J., Molina-Gonzalez, I., Davtyan, H., Lodge, R.J., Glover, J.D., Wallace, R., Munro, D.A.D., David, E., Amit, I., Miron, V.E., Priller, J., Jenkins, S.J., Hardingham, G.E., Blurton-Jones, M., Mabbott, N.A., Summers, K.M., Hohenstein, P., Hume, D.A., Pridans, C., 2019. Deletion of a Csf1r enhancer selectively impacts CSF1R expression and

development of tissue macrophage populations. Nat Commun 10, 3215. https://doi.org/10.1038/s41467-019-11053-8

Rowlands, D., Lensjø, K.K., Dinh, T., Yang, S., Andrews, M.R., Hafting, T., Fyhn, M., Fawcett, J.W., Dick, G., 2018. Aggrecan Directs Extracellular Matrix-Mediated Neuronal Plasticity. J Neurosci 38, 10102–10113. https://doi.org/10.1523/JNEUROSCI.1122-18.2018

Saupe, F., Schwenzer, A., Jia, Y., Gasser, I., Spenlé, C., Langlois, B., Kammerer, M., Lefebvre, O., Hlushchuk, R., Rupp, T., Marko, M., van der Heyden, M., Cremel, G., Arnold, C., Klein, A., Simon-Assmann, P., Djonov, V., Neuville-Méchine, A., Esposito, I., Slotta-Huspenina, J., Janssen, K.-P., de Wever, O., Christofori, G., Hussenet, T., Orend, G., 2013. Tenascin-C Downregulates Wnt Inhibitor Dickkopf-1, Promoting Tumorigenesis in a Neuroendocrine Tumor Model. Cell Reports 5, 482–492. https://doi.org/10.1016/j.celrep.2013.09.014

Schafer, D.P., Lehrman, E.K., Kautzman, A.G., Koyama, R., Mardinly, A.R., Yamasaki, R., Ransohoff, R.M., Greenberg, M.E., Barres, B.A., Stevens, B., 2012. Microglia Sculpt Postnatal Neural Circuits in an Activity and Complement-Dependent Manner. Neuron 74, 691–705. https://doi.org/10.1016/j.neuron.2012.03.026

Schwabe, T., Srinivasan, K., Rhinn, H., 2020. Shifting paradigms: The central role of microglia in Alzheimer's disease. Neurobiology of Disease 143, 104962. https://doi.org/10.1016/j.nbd.2020.104962

Shao, X., Gomez, C.D., Kapoor, N., Considine, J.M., Grams, C., Gao, Y.T., Naba, A., 2023. MatrisomeDB 2.0: 2023 updates to the ECM-protein knowledge database. Nucleic Acids Res 51, D1519–D1530. https://doi.org/10.1093/nar/gkac1009

Soles, A., Selimovic, A., Sbrocco, K., Ghannoum, F., Hamel, K., Moncada, E.L., Gilliat, S., Cvetanovic, M., 2023. Extracellular Matrix Regulation in Physiology and in Brain Disease. Int J Mol Sci 24, 7049. https://doi.org/10.3390/ijms24087049

Song, K.H., Park, J., Park, J.H., Natarajan, R., Ha, H., 2013. Fractalkine and its receptor mediate extracellular matrix accumulation in diabetic nephropathy in mice. Diabetologia 56, 1661–1669. https://doi.org/10.1007/s00125-013-2907-z

Sorg, B.A., Berretta, S., Blacktop, J.M., Fawcett, J.W., Kitagawa, H., Kwok, J.C.F., Miquel, M., 2016. Casting a Wide Net: Role of Perineuronal Nets in Neural Plasticity. J. Neurosci. 36, 11459–11468. https://doi.org/10.1523/JNEUROSCI.2351-16.2016

Soria, F.N., Paviolo, C., Doudnikoff, E., Arotcarena, M.-L., Lee, A., Danné, N., Mandal, A.K., Gosset, P., Dehay, B., Groc, L., Cognet, L., Bezard, E., 2020. Synucleinopathy alters nanoscale organization and diffusion in the brain extracellular space through hyaluronan remodeling. Nat Commun 11, 3440. https://doi.org/10.1038/s41467-020-17328-9

Stevens, B., Allen, N.J., Vazquez, L.E., Howell, G.R., Christopherson, K.S., Nouri, N., Micheva, K.D., Mehalow, A.K., Huberman, A.D., Stafford, B., Sher, A., Litke, A.M., Lambris, J.D., Smith, S.J., John, S.W.M., Barres, B.A., 2007. The Classical Complement Cascade Mediates CNS Synapse Elimination. Cell 131, 1164–1178. https://doi.org/10.1016/j.cell.2007.10.036

Sugitani, K., Egorova, D., Mizumoto, S., Nishio, S., Yamada, S., Kitagawa, H., Oshima, K., Nadano, D., Matsuda, T., Miyata, S., 2021. Hyaluronan degradation and release of a hyaluronan-aggrecan complex from perineuronal nets in the aged mouse brain. Biochimica et Biophysica Acta (BBA) - General Subjects 1865, 129804. https://doi.org/10.1016/j.bbagen.2020.129804

Suttkus, A., Rohn, S., Weigel, S., Glöckner, P., Arendt, T., Morawski, M., 2014. Aggrecan, link protein and tenascin-R are essential components of the perineuronal net to protect neurons against iron-induced oxidative stress. Cell Death Dis 5, e1119–e1119. https://doi.org/10.1038/cddis.2014.25

Tagliaferro, P., Burke, R.E., 2016. Retrograde Axonal Degeneration in Parkinson Disease. Journal of Parkinson's Disease 6, 1–15. https://doi.org/10.3233/JPD-150769

Tavianatou, A.G., Caon, I., Franchi, M., Piperigkou, Z., Galesso, D., Karamanos, N.K., 2019. Hyaluronan: molecular size-dependent signaling and biological functions in inflammation and cancer. The FEBS Journal 286, 2883–2908. https://doi.org/10.1111/febs.14777

Terry, R.D., Masliah, E., Salmon, D.P., Butters, N., DeTeresa, R., Hill, R., Hansen, L.A., Katzman, R., 1991. Physical basis of cognitive alterations in alzheimer's disease: Synapse loss is the major correlate of cognitive impairment. Annals of Neurology 30, 572–580. https://doi.org/10.1002/ana.410300410

Tewari, B.P., Chaunsali, L., Prim, C.E., Sontheimer, H., 2022. A glial perspective on the extracellular matrix and perineuronal net remodeling in the central nervous system. Front Cell Neurosci 16, 1022754. https://doi.org/10.3389/fncel.2022.1022754

Ueno, H., Fujii, K., Takao, K., Suemitsu, S., Murakami, S., Kitamura, N., Wani, K., Matsumoto, Y., Okamoto, M., Ishihara, T., 2019. Alteration of parvalbumin expression and perineuronal nets formation in the cerebral cortex of aged mice. Molecular and Cellular Neuroscience 95, 31–42. https://doi.org/10.1016/j.mcn.2018.12.008

Ueno, H., Takao, K., Suemitsu, S., Murakami, S., Kitamura, N., Wani, K., Okamoto, M., Aoki, S., Ishihara, T., 2018. Age-dependent and region-specific alteration of parvalbumin neurons and perineuronal nets in the mouse cerebral cortex. Neurochemistry International 112, 59–70. https://doi.org/10.1016/j.neuint.2017.11.001

Venturino, A., Schulz, R., De Jesús-Cortés, H., Maes, M.E., Nagy, B., Reilly-Andújar, F., Colombo, G., Cubero, R.J.A., Schoot Uiterkamp, F.E., Bear, M.F., Siegert, S., 2021. Microglia enable mature perineuronal nets disassembly upon anesthetic ketamine exposure or 60-Hz light entrainment in the healthy brain. Cell Reports 36, 109313. https://doi.org/10.1016/j.celrep.2021.109313

Verheggen, I.C.M., de Jong, J.J.A., van Boxtel, M.P.J., Gronenschild, E.H.B.M., Palm, W.M., Postma, A.A., Jansen, J.F.A., Verhey, F.R.J., Backes, W.H., 2020. Increase in blood–brain barrier leakage in healthy, older adults. GeroScience 42, 1183–1193. https://doi.org/10.1007/s11357-020-00211-2

Wang, Q., Wang, C., Ji, B., Zhou, J., Yang, C., Chen, J., 2019. Hapln2 in Neurological Diseases and Its Potential as Therapeutic Target. Frontiers in Aging Neuroscience 11, 60. https://doi.org/10.3389/fnagi.2019.00060

Weber, P., Bartsch, U., Rasband, M.N., Czaniera, R., Lang, Y., Bluethmann, H., Margolis, R.U., Levinson, S.R., Shrager, P., Montag, D., Schachner, M., 1999. Mice Deficient for Tenascin-R Display Alterations of the Extracellular Matrix and Decreased Axonal Conduction Velocities in the CNS. J. Neurosci. 19, 4245–4262. https://doi.org/10.1523/JNEUROSCI.19-11-04245.1999

Weinhard, L., di Bartolomei, G., Bolasco, G., Machado, P., Schieber, N.L., Neniskyte, U., Exiga, M., Vadisiute, A., Raggioli, A., Schertel, A., Schwab, Y., Gross, C.T., 2018. Microglia remodel synapses by presynaptic trogocytosis and spine head filopodia induction. Nat Commun 9, 1228. https://doi.org/10.1038/s41467-018-03566-5

Wilson, E., Knudson, W., Newell-Litwa, K., 2020. Hyaluronan regulates synapse formation and function in developing neural networks. Sci Rep 10, 16459. https://doi.org/10.1038/s41598-020-73177-y

Wilson, I.A., Ikonen, S., Gallagher, M., Eichenbaum, H., Tanila, H., 2005. Age-Associated Alterations of Hippocampal Place Cells Are Subregion Specific. J. Neurosci. 25, 6877–6886. https://doi.org/10.1523/JNEUROSCI.1744-05.2005

Wilton, D.K., Mastro, K., Heller, M.D., Gergits, F.W., Willing, C.R., Fahey, J.B., Frouin, A., Daggett, A., Gu, X., Kim, Y.A., Faull, R.L.M., Jayadev, S., Yednock, T., Yang, X.W., Stevens, B., 2023. Microglia and complement mediate early corticostriatal synapse loss and cognitive dysfunction in Huntington's disease. Nat Med 29, 2866–2884. https://doi.org/10.1038/s41591-023-02566-3

Wood, H., 2022. α-Synuclein-activated microglia are implicated in PD pathogenesis. Nat Rev Neurol 18, 188–188. https://doi.org/10.1038/s41582-022-00631-y

Zhang, Y., Chen, K., Sloan, S.A., Bennett, M.L., Scholze, A.R., O'Keeffe, S., Phatnani, H.P., Guarnieri, P., Caneda, C., Ruderisch, N., Deng, S., Liddelow, S.A., Zhang, C., Daneman, R., Maniatis, T., Barres, B.A., Wu, J.Q., 2014. An RNA-Sequencing Transcriptome and Splicing Database of Glia, Neurons, and Vascular Cells of the Cerebral Cortex. J. Neurosci. 34, 11929–11947. https://doi.org/10.1523/JNEUROSCI.1860-14.2014

Zheng, Q., Liu, H., Yu, W., Dong, Y., Zhou, L., Deng, W., Hua, F., 2023. Mechanical properties of the brain: Focus on the essential role of Piezo1-mediated mechanotransduction in the CNS. Brain and Behavior 13. https://doi.org/10.1002/brb3.3136

Zhou, Y., Zhou, B., Pache, L., Chang, M., Khodabakhshi, A.H., Tanaseichuk, O., Benner, C., Chanda, S.K., 2019. Metascape provides a biologist-oriented resource for the analysis of systems-level datasets. Nat Commun 10, 1523. https://doi.org/10.1038/s41467-019-09234-6

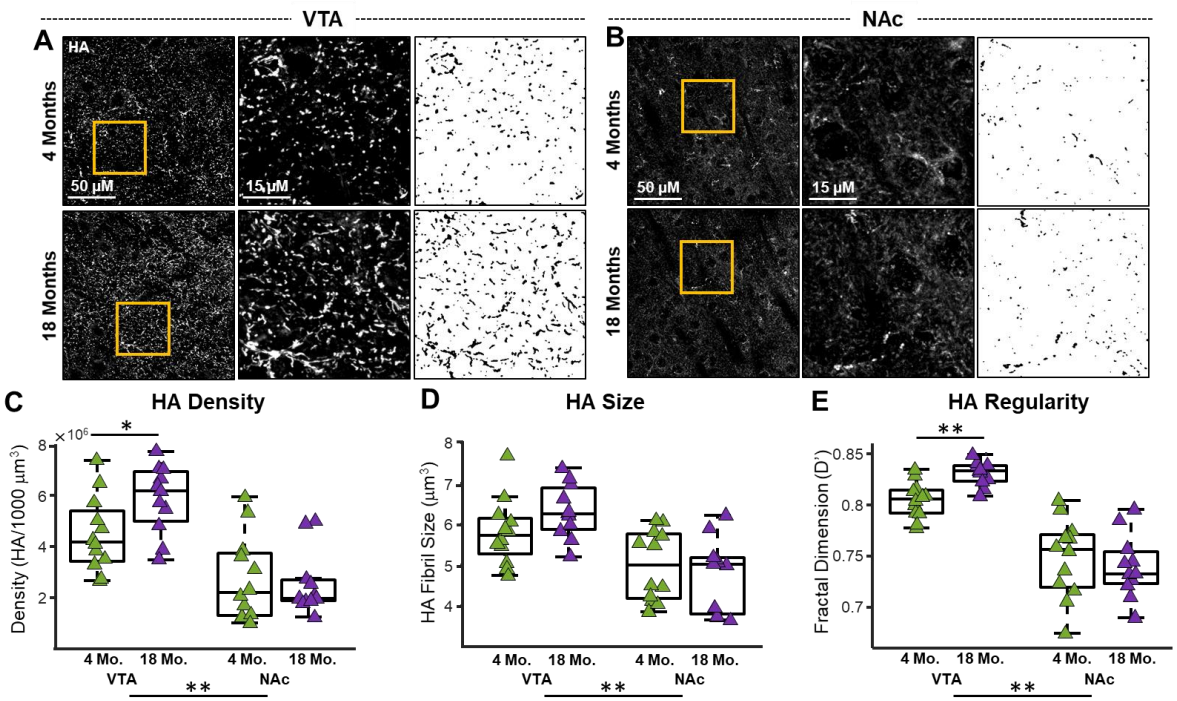

Figure 1. Increased hyaluronan matrix deposition in the ventral tegmental area (VTA) of aging wild-type mice. **A)** Example photomicrographs of histochemically labelled hyaluronan (HA) in the VTA and **B)** nucleus accumbens (NAc) of a young adult (4 months) and late-middle-aged (18 months) mouse (left panels). Middle panels show zoomed in images of the areas within the yellow squares in the left panels. The right panels depict binarized images of the hyaluronan matrix used for quantification. **C)** The density of hyaluronan fibrils detected in the VTA and NAc of young-adult (green) and aged (purple) mice. **D)** Median hyaluronan fibril sizes in the VTA and NAc of the same mice. **E)** Measurements of hyaluronan distribution regularity assessed using the Fractal Dimension plugin in Fiji image analysis software. Higher fractal dimension values (D') indicate more regularity in the hyaluronan matrix. * $p < 0.05$; ** $p < 0.01$.

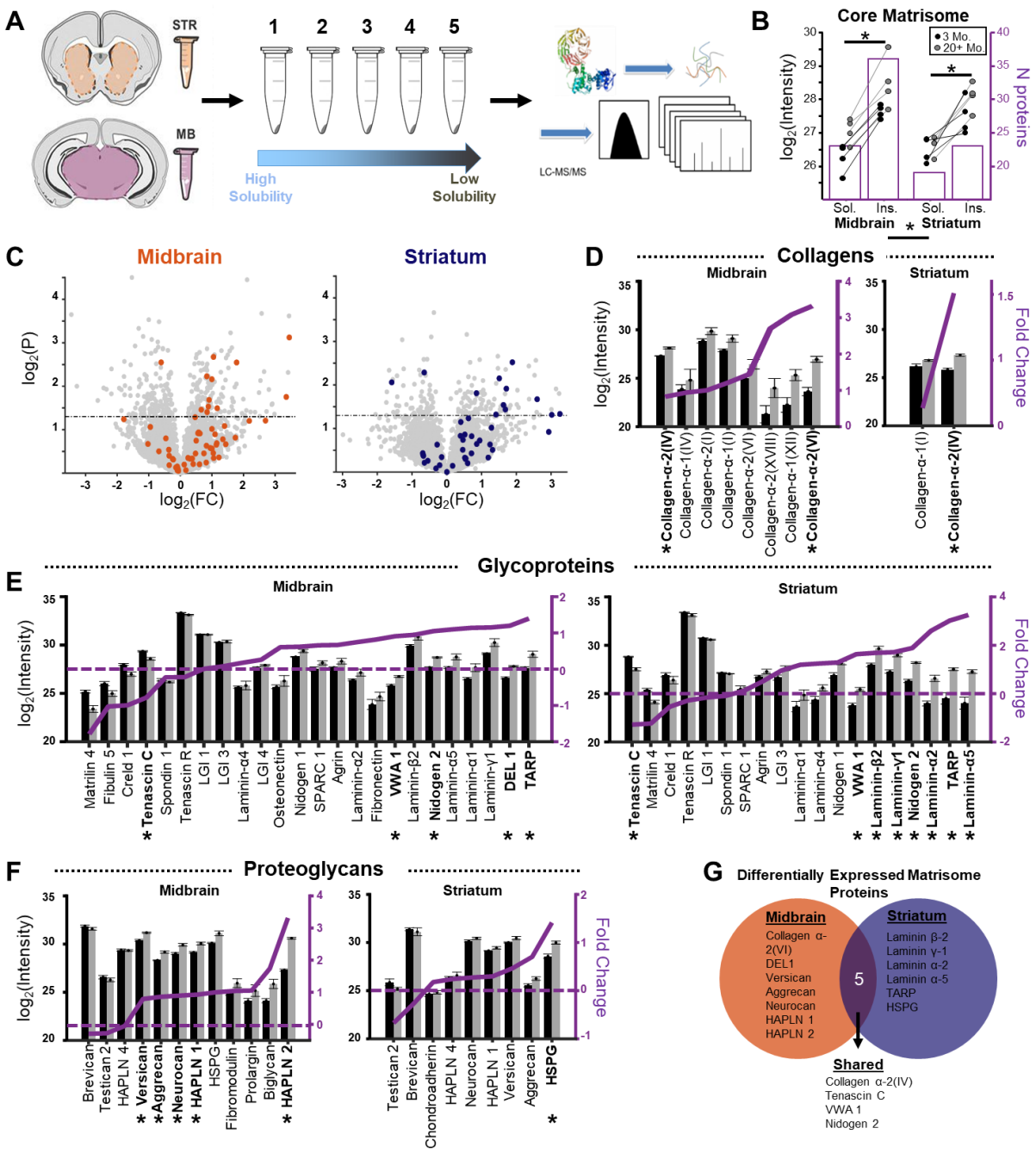

Figure 2. Proteomic mapping of age-associated changes in midbrain and striatum core matrisome protein abundances reveals key regional differences. **A)** Schematic of the proteomic workflow. The midbrain and striatum of young adult (3-4 months) and aged (20-24 months) wild-type mice were dissected out. Tissue underwent a fractionation protocol that yielded multiple samples of proteins with decreasing solubility, and a final insoluble pellet. All samples were then

sent for liquid chromatography with tandem mass spectrometry (LC-MS/MS) analysis. **B)** The average log2-transformed intensity values of all core matrisome proteins detected in the soluble and insoluble midbrain and striatum samples (black axis on left). Black dots represent the individual young-adult animals and grey dots represent the aged mice. The purple bars denote the number of core matrisome proteins detected in the soluble and insoluble fractions for each region (purple axis on right). **C)** Volcano plots of all proteins pooled across fractions for the midbrain and striatum. The orange and blue dots denote individual core matrisome proteins detected in each region. Fold-changes were calculated with respect to the aged mice (positive values indicate greater with age). **D)** Log2-transformed intensity values (black axis on left) and fold changes (purple axis on right) for all collagens detected in the midbrain and striatum of young (black) and aged (grey) mice. **E)** Abundances and fold changes for all detected glycoproteins in the midbrain and striatum. Figure convention as in **D**. Dotted purple line represents a fold-change of 0. **F)** Abundance and fold changes for all detected proteoglycans in the midbrain and striatum. Figure convention as in **E**. **G)** Venn diagram depicting all differentially expressed core matrisome proteins found specifically in the midbrain (orange), striatum (blue), as well as those differentially expressed in both regions. * $p < 0.05$

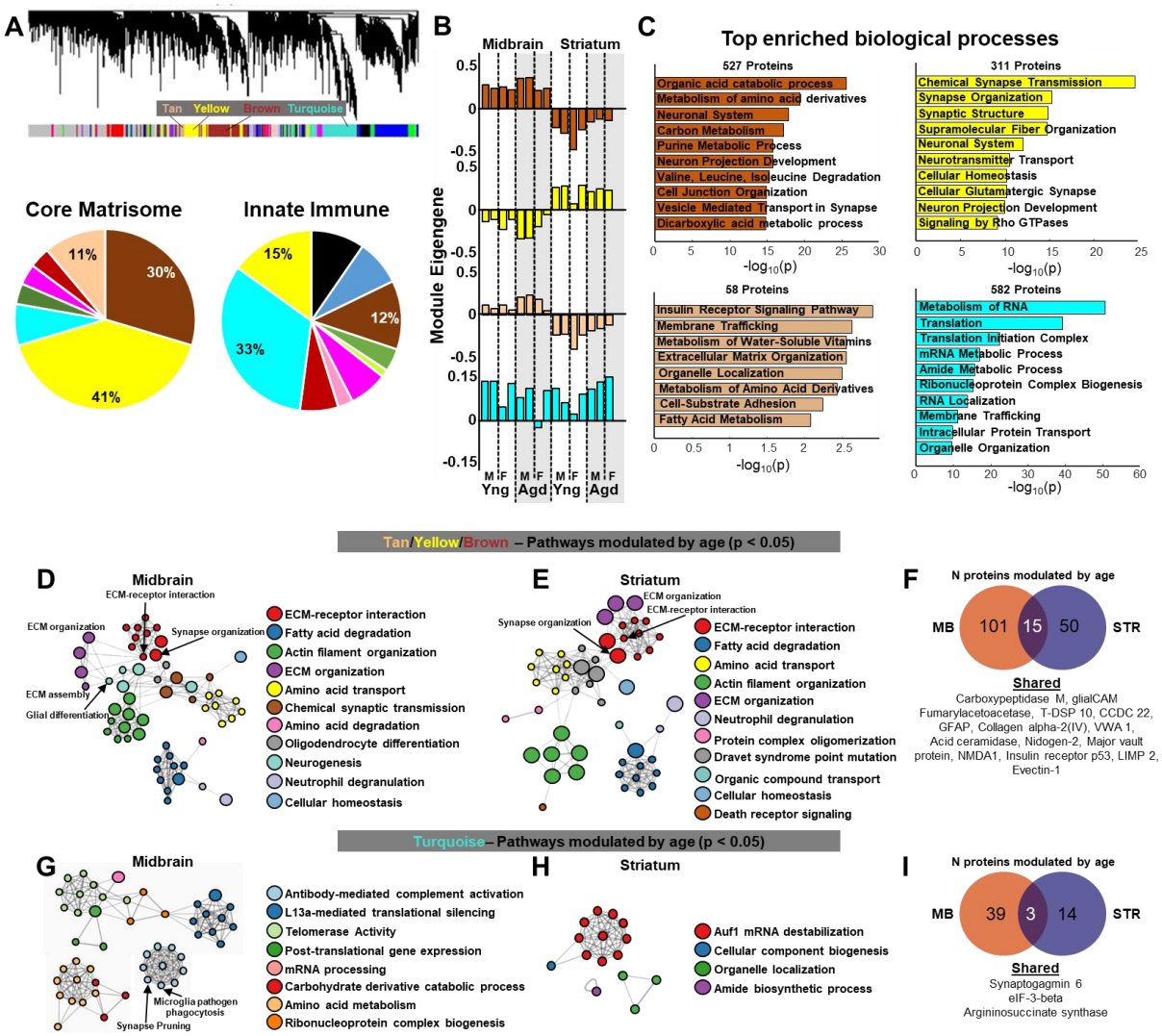

Figure 3. Weighted gene coexpression network analysis (WGCNA) of proteomic data. **A)** Top: dendrogram generated by WGCNA analysis of all midbrain and striatal proteomic samples. Bottom: pie charts of core matrisome and innate immune protein distribution across modules. Percentages were calculated as the proportion of all proteins within each class that were classified by the given module. Only percentage values above 10% are depicted. **B)** Module eigengenes for each of the 4 modules highlighted in **A** for each sample. One aged female was classified as an outlier by the WGCNA and was removed from subsequent analyses. **C)** The most enriched biological terms associated with brown, yellow, tan, and turquoise module proteins. **D)** Network plot of process and pathway enrichment terms associated with all

tan/yellow/brown module proteins whose abundances were modulated by age ($p<0.05$) in the midbrain and **E**) striatum. Various terms associated with ECM organization, synapse organization, and glial differentiation are highlighted with black arrows. **F)** Venn diagram depicting the number of tan/yellow/brown module proteins modulated by age in the midbrain (orange) and striatum (blue), as well as those differentially expressed in both regions. **G)** Network plot of process and pathway enrichment terms associated with all turquoise module proteins whose abundances were modulated by age ($p<0.05$) in the midbrain and **H)** striatum. Microglia pathogen phagocytosis and synapse pruning terms that were part of a larger group of terms associated with antibody-mediated complement activation are highlighted with black arrows. **I)** Venn diagram depicting the number of turquoise module proteins modulated by age in the midbrain (orange) and striatum (blue), as well as those differentially expressed in both regions.

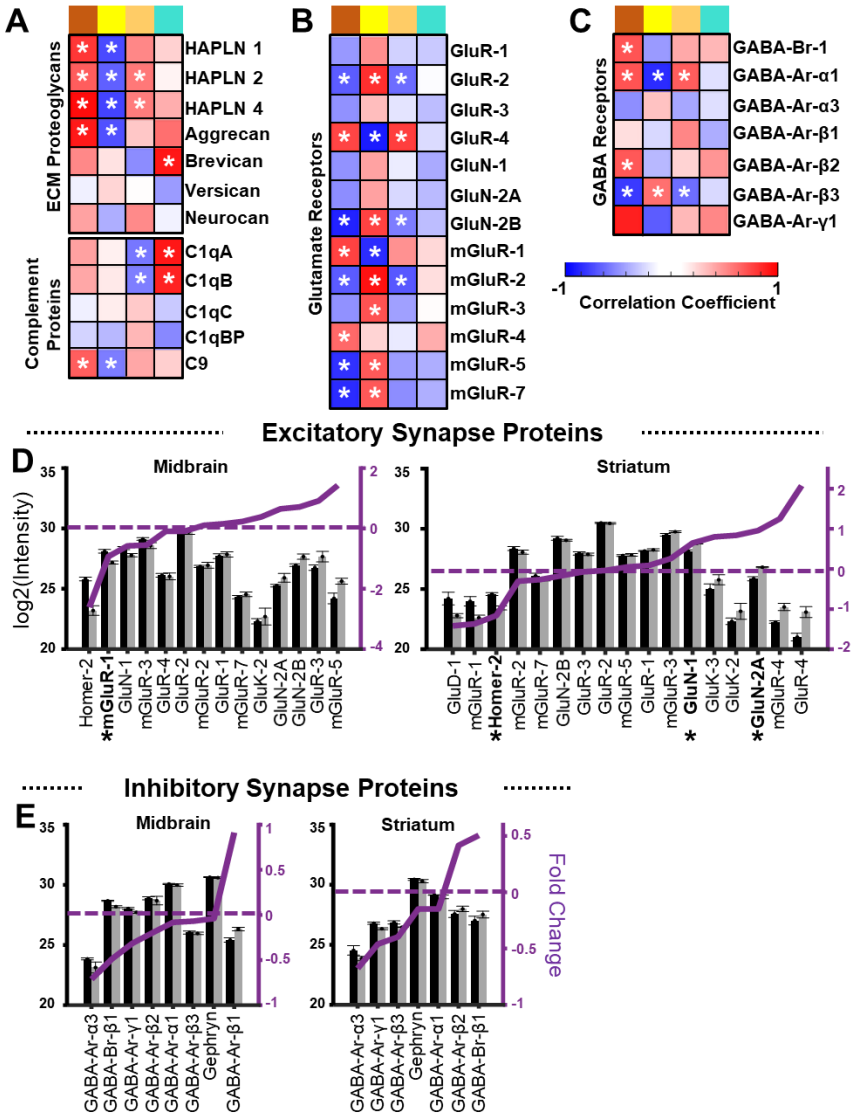

Figure 4. Synapse status is associated with ECM proteoglycan abundance in the aging mesolimbic dopamine system. **A)** Heatmaps representing correlations between brown, yellow, tan, and turquoise module eigengenes and extracellular matrix proteoglycan and complement protein abundances. **B)** Heatmaps representing correlations between the same module eigengenes and glutamatergic and **C)** GABAergic synapse receptor abundances. **D)** Log2-transformed intensity values (black axis on left) and fold changes (purple axis on right) for all excitatory synapse and **E)** inhibitory proteins detected in the midbrain and striatum of young (black) and aged (grey) mice. The dotted purple line represents a fold-change of 0. * $p < 0.05$

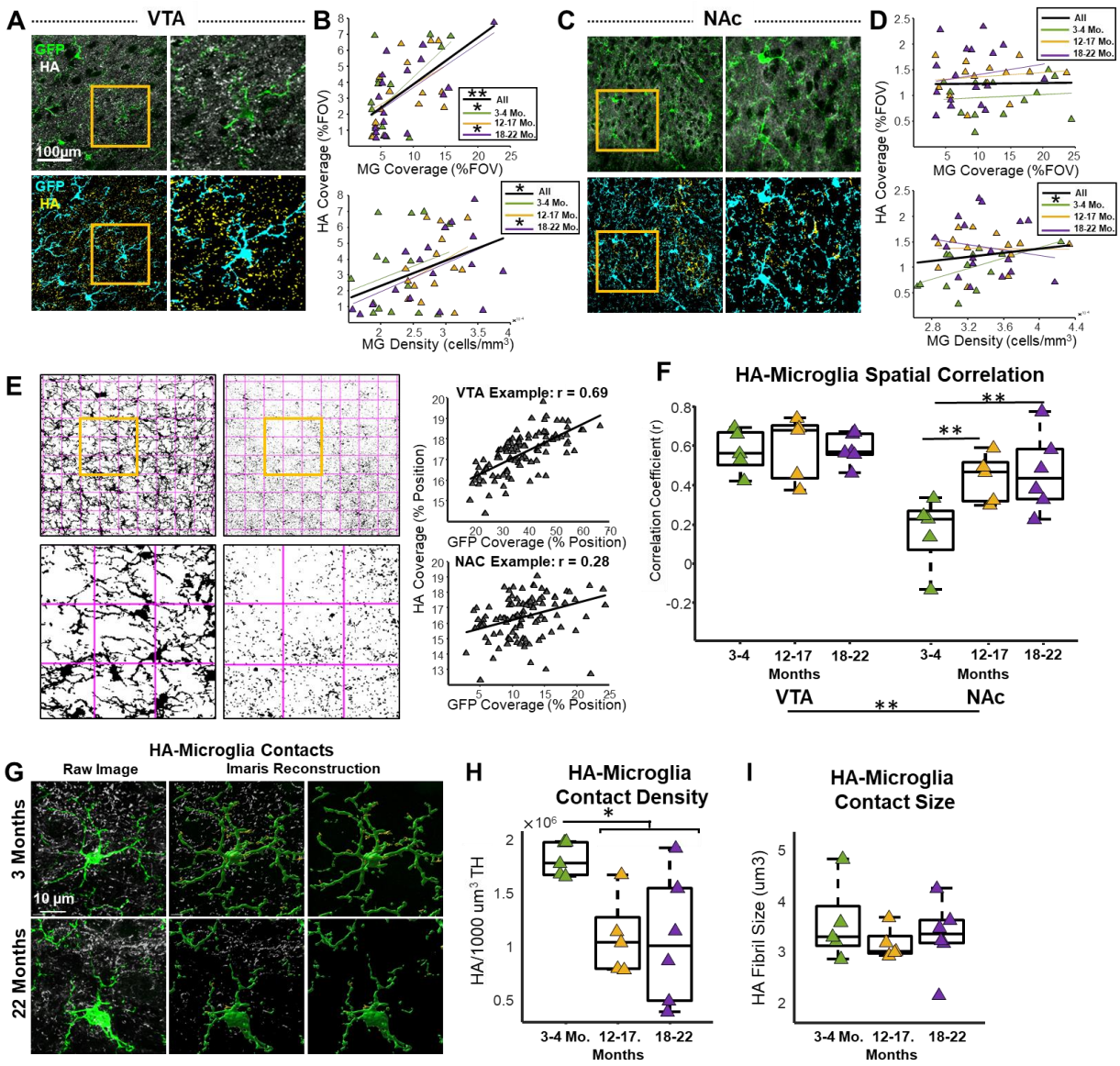

Figure 5. Spatial relationships between microglial tissue coverage and the hyaluronan matrix. **A)** Top row: example photomicrograph of 20x confocal images of histochemically labelled hyaluronan (HA) and GFP-labelled microglia from the ventral tegmental area (VTA) of a young-adult (3 months) Cx3Cr1$^{EGFP/+}$ mouse. The image in the left panel is a zoom in on the field of view depicted by the yellow square on the right. Bottom row: threshold images of the hyaluronan and GFP signals used for analysis. Again, the image in the left panel is a zoom in on the field of view depicted by the yellow square on the right. **B)** Scatter plots of VTA hyaluronan field of view

tissue coverage (% FOV) against field-of-view microglial tissue coverage (top) and microglial densities (bottom) for young-adult (3-4 months; green), middle-aged (12-17 months; yellow), and aged (18-22 months; purple) Cx3Cr1$^{EGFP/+}$ mice. The black line is the trend line of the relationships when all mice are assessed together, the green for young-adult mice, yellow for middle-aged mice, and purple for aged mice. Asterisks in the legends depict significant correlations as assessed by linear regression analysis. **C)** Example photomicrograph of 20x confocal images of histochemically labelled hyaluronan (HA) and GFP-labelled microglia from the nucleus accumbens (NAc) of a young-adult (3 months) Cx3Cr1$^{EGFP/+}$ mouse. Image conventions as in **A**. **D)** Scatter plots of NAc hyaluronan field of view tissue coverage (% FOV) against field-of-view microglial tissue coverage (top) and microglial densities (bottom) in the same mice. Image conventions as in **B**. **E)** Left: example of grid overlaid on 20x confocal images to determine spatial correlations between hyaluronan and GFP signals. Images on the bottom are zoom-ins of the areas depicted by the yellow squares on the top. Right: The Pearson's correlation coefficient was calculated for each image by correlating the hyaluronan and GFP signals within each square. The top scatter plot is an example from the VTA and the bottom from the NAc. **F**) Correlation coefficients of spatial relationships between hyaluronan and microglia in the VTA and NAc for young-adult, middle-aged and aged mice. Boxplots denote the middle 50% of the data and horizontal lines denote the median of each distribution. **G)** Left panel: example 63x photomicrographs of GFP-positive VTA microglia and hyaluronan from 3- and 22-month-old Cx3Cr1$^{EGFP/+}$ mice. Middle and right panels: Imaris reconstructions of microglia and hyaluronan followed by filtering for hyaluronan fibrils contacted by microglia. **H)** The density of hyaluronan fibrils in contact with microglia normalized by the total volume of the GFP signal for young, middle-aged, and aged mice. **I)** The median size of hyaluronan fibrils in contact with microglia for the same mice. Boxplots denote the middle 50% of the data and horizontal lines denote the median of each distribution. * $p < 0.05$; ** $p < 0.01$.

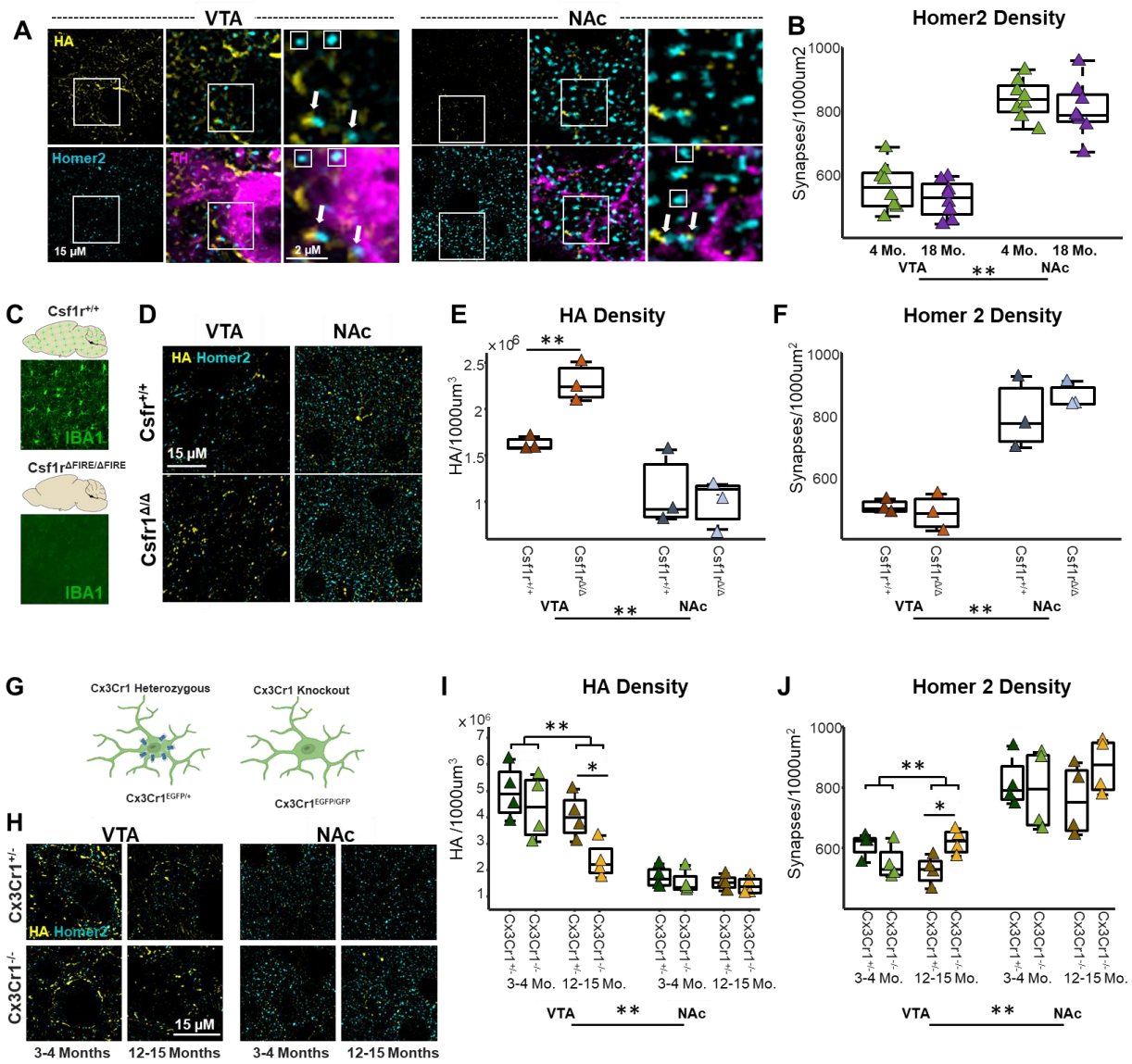

Figure 6. Microglia modulate hyaluronan and synapse abundances in the aging mesolimbic dopamine system. **A)** Example photomicrographs of histochemically labelled hyaluronan and immunohistochemically labelled Homer2 (excitatory synapses) and tyrosine hydroxylase (TH; dopaminergic neurons/processes) in the VTA and NAc of a young-adult wild-type mouse. Middle panels are zoomed in images of the fields of view depicted in the white squares in the left panels, and the right panels are the zoomed in images of the fields of view depicted by the white squares in the middle panels. Arrows highlight putative hyaluronan-Homer2 colocalized puncta and small squares depict Homer2 puncta not associated with the hyaluronan matrix. **B)**

Homer2 puncta densities in the VTA and NAc of young-adult and middle-aged mice. Boxplots denote the middle 50% of the data and horizontal lines denote the median of each distribution. **C)** Staining for IBA1-positive microglia confirmed constitutive depletion of microglia in $Csf1r^{\Delta FIRE/\Delta FIRE}$ mice (photomicrographs), but not in $Csf1r^{+/+}$ mice. **D)** Example photomicrographs of histochemically labelled hyaluronan and immunohistochemically labelled Homer2 from the VTA and NAc of $Csf1r^{+/+}$ and $Csf1r^{\Delta FIRE/\Delta FIRE}$ mice. **E)** Hyaluronan fibril densities in the VTA (orange) and NAc (blue) of $Csf1r^{+/+}$(darker triangles) and $Csf1r^{\Delta FIRE/\Delta FIRE}$ (lighter triangles) mice. **F)** Homer2 puncta densities in the VTA and NAc of $Csf1r^{+/+}$ and $Csf1r^{\Delta FIRE/\Delta FIRE}$ mice. **G)** Tissue from Cx3Cr1-deficient ($Cx3Cr1^{EGFP/+}$) and Cx3Cr1-knockout ($Cx3Cr1^{EGFP/EGFP}$) mice was histologically examined. **H)** Images show example photomicrographs of histochemically labelled hyaluronan and immunohistochemically labelled Homer2 in the VTA and NAc of young-adult (3-4 months) and middle-aged (12-15 months) $Cx3Cr1^{EGFP/+}$ and $Cx3Cr1^{EGFP/EGFP}$ mice. **I)** Hyaluronan fibril densities in the VTA and NAc of $Cx3Cr1^{EGFP/+}$ (darker triangles) and $Cx3Cr1^{EGFP/EGFP}$ (lighter triangles) mice. **J)** Homer2 puncta densities in the VTA and NAc of $Cx3Cr1^{EGFP/+}$ and $Cx3Cr1^{EGFP/EGFP}$ mice. * $p < 0.05$; ** $p < 0.01$.